

Contents lists available at ScienceDirect

Tectonophysics

journal homepage: www.elsevier.com/locate/tecto



Segmentation in continental forearcs: Links between large-scale overriding plate structure and seismogenic behavior associated with the 2010 M_w 8.8 Maule, Chile earthquake



Brandon T. Bishop^{a,*}, Susan L. Beck^b, George Zandt^b

- a Department of Earth and Atmospheric Sciences, Saint Louis University, 3642 Lindell Boulevard, Saint Louis, MO 63108, USA
- ^b Department of Geosciences, University of Arizona, 1040 East 4th Street, Tucson, AZ 85721, USA

ARTICLE INFO

Keywords: Subduction Megathrust Forearc Chilean Trench Maule Earthquake Receiver Function

ABSTRACT

Subduction along the active margin of a continental plate occurs in a context where the overriding plate's crust and lithospheric mantle may contain inherited structures significantly predating the present tectonic conditions of the margin. These structures are persistent over very long-term time scales (> 10^5 to > 10^6 years) and are thought to play an important role in both seismogenic processes on the megathrust and development of topography along coastlines. We use receiver functions calculated from broadband seismic data collected along the Chilean forearc between ~33°S and 38.5°S in the vicinity of the 2010 M_w 8.8 Maule earthquake to determine the structure of the overriding South American continental plate and subducting Nazca oceanic plate along and inboard of the seismogenic portion of the megathrust. We show that the Chilean forearc is divided into three structurally distinct zones: a northern zone where the continental crust intersects the subducting plate well inboard of the coast at ~35–40 km depth, a central zone where the continental crust tapers to < 20 km thickness at the coast before intersecting the subducting plate at 15–20 km depth, and a southern zone corresponding approximately to the rapidly uplifting Arauco Peninsula where we find that the continental crust forms a wedge-shaped feature ~35–40 km in thickness which intersects the subducting plate well inboard of the coast. The thin crust of the central zone is associated with a dense, high velocity mantle body (the Cobquecura anomaly) that may have played an important role in stabilizing this segment of the Chilean forearc since the late Paleozoic.

1. Introduction

The forearc and subduction zone in central Chile (Fig. 1) represent a transition between the accreting active margin of southern Chile and the erosive active margin of northern Chile separated by the subducting Juan Fernandez Ridge at $\sim\!33^\circ\mathrm{S}$ (e.g. Clift and Vannucchi, 2004; Contreras-Reyes et al., 2010). The forearc south of $\sim\!34^\circ\mathrm{S}\!-\!35^\circ\mathrm{S}$ exposes $\sim\!275\,\mathrm{Myr}$ to $\sim\!300\,\mathrm{Myr}$ old pre-Andean subduction complex structures (including a paired metamorphic belt, intruding Carboniferous-age batholith, and set of left lateral strike-slip faults inactive since $\sim\!275\,\mathrm{Ma}$) at the present coastline, indicating that the margin has overall been largely stable for much of the Mesozoic and Cenozoic (Hervé, 1988; Glodny et al., 2008a; Willner et al., 2009; Hervé et al., 2013; see also Charrier et al., 2007 for broader overview). In this study we investigate the possible lithospheric-scale expression of these persistent structures and their potential to affect seismogenic processes on the megathrust in central Chile and on coastal uplift over $>100\,\mathrm{kyr}$

to > 1 Myr time scales along the segment of the central Chilean megathrust that ruptured during the 27 February 2010 Maule earthquake originating near 36°S (Fig. 1A, Duputel et al., 2012).

The great 27 February 2010 Maule earthquake was an $8.8\,\mathrm{M}_W$ event that ruptured a section of the locked megathrust zone (Fig. 1B) spanning an along-strike length of $\sim 500\,\mathrm{km}$ to a depth of 40 to $50\,\mathrm{km}$ (Fig. 1C). Multiple analyses of the 2010 Maule earthquake have shown that the event ruptured bilaterally and that the greatest magnitude of slip was concentrated in 2 to 3 patches (dark blue features in Fig. 1D). The highest slip patch (> 15 m of co-seismic slip) occurs offshore north of the hypocenter (Delouis et al., 2010; Kiser and Ishii, 2011; Lorito et al., 2011; Koper et al., 2012; Moreno et al., 2012; Yue et al., 2014: Huang et al., 2017). The second, lower magnitude region of slip occurred south of the hypocenter. Different studies have determined varying amounts of co-seismic slip in this region (Delouis et al., 2010; Lorito et al., 2011; Koper et al., 2012; Moreno et al., 2012; Yue et al., 2014; Huang et al., 2017). These studies indicate that the hypocentral

E-mail address: brandon.t.bishop@slu.edu (B.T. Bishop).

^{*} Corresponding author.

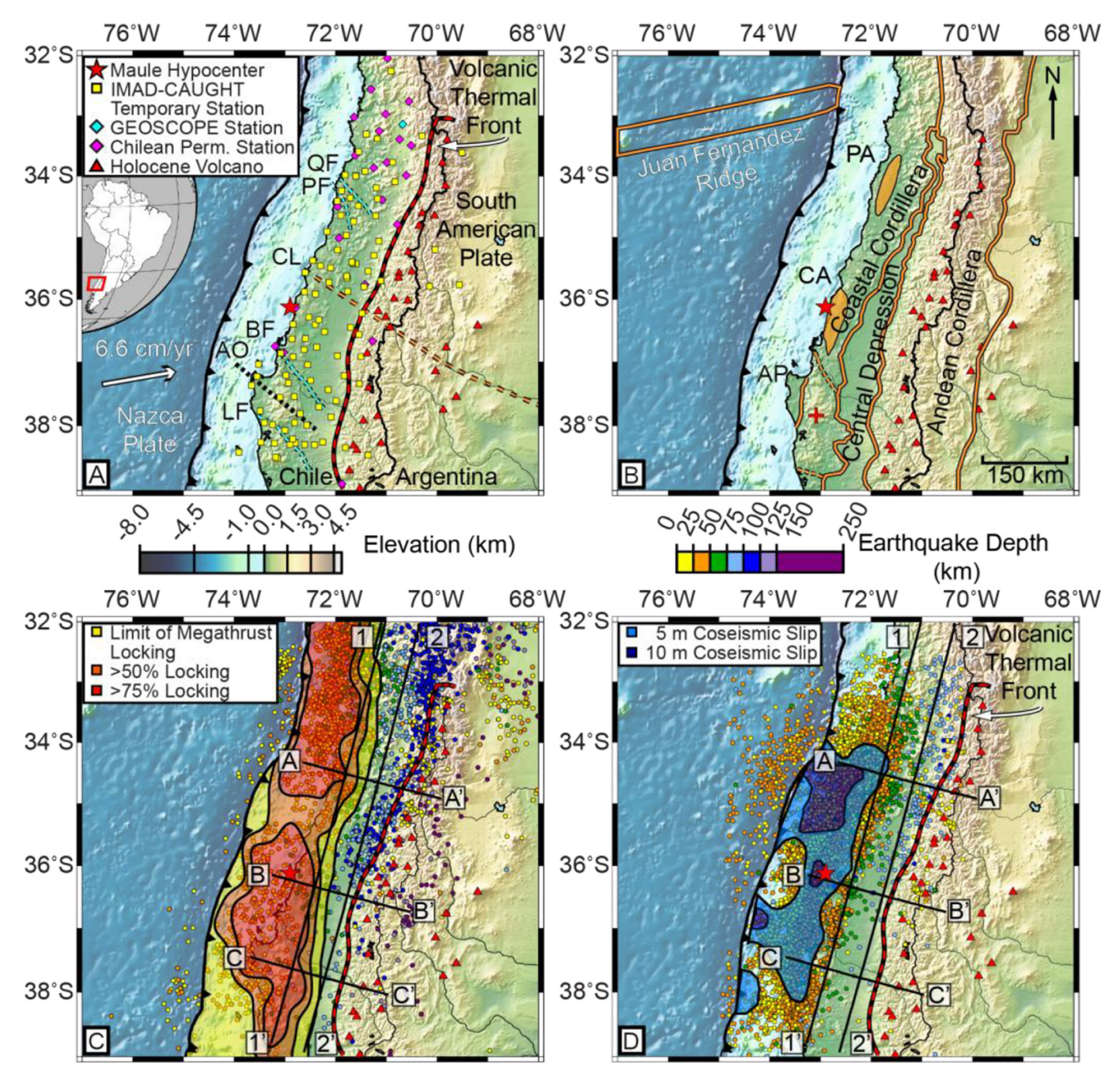


Fig. 1. Maule segment of central Chile. A. Location of seismic stations used in this study and major upper plate faults and lineaments along with inset map showing study location with respect to South America. Arrow marks orientation of Nazca plate motion with respect to South America (Kendrick et al., 2003). Dashed red line VTF (volcanic thermal front) marks the location of the high lateral thermal gradient associated with the arc extrapolated from Völker and Stipp (2015) forearc thermal model. Dashed black lines mark axes of Arauco Orocline associated with the Arauco Peninsula and adjacent section of the Coastal Cordillera (after Jara-Muñoz et al., 2015). Dashed cyan lines mark significant forearc faults discussed in the text (OF - Quebrada Honda/Topocalma fault system, PF- Pichilemu fault system, BF - Bio-Bio Fault, LF - Lanalhue Fault (after Jara-Muñoz et al., 2015 and Aron et al., 2015)). Dashed orange line CL marks Cortaderas Lineament (modified from Ramos and Kay, 2006, see sections 4.1 and 4.3 for discussion). Barbed black line marks Chilean Trench. B. Geomorphic provinces in central Chile (modified from Ramos and Kay, 2006; Farías et al., 2010a; Rehak et al., 2008) and the Pichilemu (orange oval PA) and Cobquecura (orange oval CA) forearc high seismic velocity anomalies (Hicks et al., 2014); The Arauco Peninsula (AP) and adjacent segment of Coastal Cordillera (red plus-sign) mark the location of rapid uplift (from Glodny et al., 2008a; Rehak et al., 2008; Jara-Muñoz et al., 2015). C. Locations of RF cross-sections used in this study (see section 3 for discussion) and ≥4.5 M hypocenter locations from the NEIC (1970 to December 1, 2016, excluding events from the day of the Maule 8.8 Mw earthquake to one year after). Teal, purple and pink contours represent 75%, 50%, and approximate down dip limit of pre-Maule earthquake locking for the region (modified from Moreno et al., 2010). All other symbols as in A. D. Locations of RF cross-sections used in this study and Maule aftershocks from March 15, 2010 to September 30, 2010 relocated using the IMAD network (Lange et al., 2012), note that the significant increase in forearc seismic activity relative to the long-term pattern in seismicity seen in C highlights both megathrust and upper plate faults in the region. Dark blue and light blue regions mark extent of 10 m and 5 m (approximate limit of significant coseismic slip) coseismic slip modeled for the Maule February 27, 2010 earthquake (modified from Yue et al., 2014). All other symbols as in A. (For interpretation of the references to color in this figure, the reader is referred to the web version of this article.)

region experienced relatively low co-seismic slip and most rupture models generally confine the slip to the down dip part of the plate interface. Hence, the rupture can be divided into at least two or three segments, indicating that the megathrust rupture behavior within a single large earthquake varies significantly from north to south in this part of Chile.

This variability and segmentation may also be reflected in earlier large earthquakes in the region. Prior to the 2010 Maule earthquake, this region of the plate boundary failed in a series of historic earthquakes in 1835, 1928, and possibly partially in a 1906 earthquake rupture as estimated from reported damage and shaking intensity (Comte et al., 1986; Beck et al., 1998 and references therein). The $M_W = 7.9-8$ Talca 1928 earthquake occurred north of the 2010 hypocenter. The central and southern segments of the 2010 rupture zone correspond to the region last ruptured in the 1835 Concepción earthquake. The $M_w = 9.5$ Valdivia 1960 earthquake may have ruptured into the southernmost end of the 2010 event in the region of the Arauco Peninsula (Beck et al., 1998; Melnick et al., 2009). In addition, the region downdip of the 2010 hypocenter was the site of the 80-100 km depth slab intraplate Chillan earthquake in 1939 that killed ~30,000 people (Beck et al., 1998). Collectively, these events indicate that this part of the plate boundary has variable rupture segmentation between earthquake cycles.

These rupture segments appear to correspond in part to two high seismic velocity anomalies imaged within the upper plate by local earthquake seismic tomography (Hicks et al., 2012; Hicks et al., 2014). The observation of these rupture segments and their correspondence between geophysical, geological, and geomorphic features have led to interest in the potential role of inherited structures on subduction zone processes and segmentation over multiple earthquake cycles (e.g. Hicks et al., 2014; Jara-Muñoz et al., 2015; Saillard et al., 2017). In order to better understand the role of inherited structures on plate boundary segmentation, we present new teleseismic receiver function (RF) results for the Chilean forearc between ~33°S and ~38.5°S covering the length of the forearc that ruptured during the 2010 Maule earthquake and extending from the coast to the active volcanic arc (see Fig. 1 for volcanic centers (Global Volcanism Program (2013)). We use these results to identify large-scale forearc structures and explore their possible relationship to long-term subduction segmentation.

While a number of geophysical studies have focused on the Maule region following the 2010 earthquake, most have either examined relatively large-scale aspects of the earthquake rupture itself or examined the marine forearc. Many studies have worked to understand processes related to megathrust rupture propagation (Delouis et al., 2010; Kiser and Ishii, 2011; Lorito et al., 2011; Koper et al., 2012; Moreno et al., 2012; Yue et al., 2014; Huang et al., 2017), and locking or coupling (e.g. Moreno et al., 2010; Métois et al., 2012). Others have sought to provide a better understanding of the marine forearc and determine its structure in relation to both the 2010 Maule earthquake and broader questions of subduction zone development (e.g. Contreras-Reyes et al., 2010; Becerra et al., 2013; Contreras-Reyes et al., 2017). Immediately following the 2010 event the International Maule Aftershock Deployment (IMAD, see Fig. 1A), a set of > 140 temporary stations deployed along the Chilean forearc from March 2010 to September 2010 (Roecker and Russo, 2010; Vilotte and RESIF, 2011), was used to examine the onshore part of the forearc. The resulting data set has already been used to relocate aftershocks for the 2010 earthquake (e.g. Lange et al., 2012; see Fig. 1C) and to perform local earthquake tomography (e.g. Hicks et al., 2012; Hicks et al., 2014) to better understand the megathrust and overriding plate.

We have used data from the IMAD deployment and other seismometers deployed in the region around the rupture of the 2010 Maule earthquake to calculate teleseismic RFs. We then used these RFs to provide images of the large-scale structure of the subducting Nazca oceanic plate and overriding South America continental plate in the region. RFs are sensitive to velocity contrasts across major boundaries

in the Earth at depth, making them ideal for imaging the Mohorovičić discontinuity (Moho) that marks the transition between crust and mantle rocks. By imaging the Moho of the South American continental crust and that of the subducted Nazca plate's oceanic crust, we are able to constrain the approximate position of the megathrust-continental Moho intersection—a feature that has been called upon to play an important role in models of megathrust seismogenic behavior (e.g. Kato et al., 2010; Peng and Gomberg, 2010; Gao and Wang, 2017) and in explanations of forearc deformation resulting in permanent coastal uplift (e.g. Melnick, 2016). In addition, models for long-term (> 100 kyr or > 1 Myr, much greater than the length of the earthquake cycle) forearc segmentation frequently call for the existence of large. persistent structures in the forearc of the upper plate which are likely to be reflected in the upper plate's crustal structure near the megathrust (e.g. Jara-Muñoz et al., 2015; Saillard et al., 2017; Dura et al., 2017). Our study further investigates and refines these models for this portion of the Chilean subduction zone.

Prior RF studies have only partially examined this section of the Chilean forearc, utilizing between four and eleven broadband seismic stations within the forearc (Gilbert et al., 2006; Heit et al., 2008; Dannowski et al., 2013). This has resulted in extremely limited spatial coverage of the region. Our data set utilizes > 100 temporary and permanent broadband seismic stations, providing nearly uniform coverage of the coast to approximately the western edge of the volcanic arc (see Fig. 1) with a lateral resolution of ~ 15 km, greatly improving upon prior RF studies of the region.

2. Data and methods

We have utilized the data from broadband seismic stations deployed from March to October 2010 as part of the temporary International Maule Aftershock Deployment (IMAD) (Roecker and Russo, 2010; Vilotte and RESIF, 2011) archived at the Incorporated Research Institutions for Seismology Data Management Center along with other archived broadband stations located between ~32°S and ~39°S from an October 2001 to December 2002 temporary deployment (Chile/Argentina Experiment (Beck et al., 2000)), the permanent Chilean National Seismic Network, and the permanent GEOSCOPE Network (Institut de Physique du Globe de Paris and Ecole et Observatoire des Sciences de la Terre de Strasbourg, 1982). This yielded a total of 94 IMAD, 9 Chile/Argentina Experiment, 22 Chilean National Seismic Network and the single GEOSCOPE station in this region with recorded data of sufficient quality to calculate at least one RF. To assess data quality, we first filtered our data using a bandpass filter with corner frequencies of 0.05 and 5 Hz to reduce the effects of noise, then visually inspected records for all arrivals of ≥5.0 M_W teleseismic earthquakes recorded at each station from distances of 30° to 90° for P-phase arrivals, 90° to 150° for PP-phase arrivals, and 110° to 160° for PKP-phase arrivals. We first excluded records lacking clear P-wave arrivals on all three components, records containing local earthquake arrivals within the time window of interest in addition to the teleseismic arrivals (a significant problem for the IMAD stations due to aftershock activity), and records containing clear instrument malfunction artifacts.

We then rotated the remaining seismic records to the radial-tangential-vertical (RTZ) coordinate system and used iterative time domain deconvolution (Ligorría and Ammon, 1999) to calculate P-to-S RFs using the data which passed our initial quality control evaluation. We used a Gaussian pulse width of 2.5, which acts as a low-pass filter with a corner frequency of 1.2 Hz. A corner frequency of 1.2 Hz allows us to resolve arrivals from layers with > -1 km thickness. Layers of this or greater thickness and step-function like boundaries will produce an RF pulse with a full-width at half maximum in time of ~ 1.05 s or in depth of ~ 8.5 km (assuming a basaltic layer with a P-wave velocity = 7.0 km/s and a S-wave velocity = 3.9 km/s (Vp/Vs = 1.8) or an intermediate composition layer with a P-wave velocity = 6.5 km/s and an S-wave velocity = 3.7 km/s (Vp/Vs = 1.75)).

Our calculations yielded a total of 7382 RF pairs of radial and tangential components. We then excluded all RF pairs with variance reductions of < 70% for the radial component and < 50% for the tangential component, yielding 1687 pairs of RFs. We then visually inspected all RF pairs to eliminate pairs where the majority of energy was on the tangential component, the initial radial component peak was not the largest arrival or was significantly delayed from the zero-lag time, and any pair with periodic arrivals on the radial component or with highly correlated radial and transverse arrivals. 1300 RF pairs passed our inspection and we then used the radial components to calculate common conversion point (CCP) stacks (Dueker and Sheehan, 1997; Sheehan et al., 2000) modified to migrate RFs through a 3-D velocity model (Frassetto et al., 2011; Frassetto and Thybo, 2013; Ryan et al., 2016). We used a 15 km bin spacing for CCP stacking, with an overlap of 1.25 × the bin spacing.

Uncertainty in the depth of features imaged in an RF CCP stack is largely a result of uncertainty in the velocity structure used to migrate the RFs. Because of this, the incorporation of a spatially varying 3-D velocity structure, where available, can be helpful in accurately resolving structure. For our study region, we use the ambient noise tomography S-wave velocity model of Ward et al., (2013) to 50 km depth. This model covers the entirety of our study area including the arc-ward portion that may be poorly sampled by local tomographic studies of the area (e.g. Farías et al., 2010a; Hicks et al., 2012; Hicks et al., 2014). Below between 50 and 55 km we incrementally merge the Ward et al. (2013) model into the Hicks et al. (2014) Vs model. To constrain the Pwave velocity to S-wave velocity ratio (Vp/Vs), we utilize the best fit 1-D Vp/Vs structure reported by Hicks et al. (2014) based on local earthquake tomography. The model then incrementally merges into the AK135 1-D global velocity model below 80 km depth. We finally note that Ward et al.'s (2013) S-wave model was calculated assuming a uniform Vp/Vs model. Ward et al.'s (2013) uncertainty estimates which varied the starting parameters (including Vp/Vs) for this S-wave model show changes of at most \sim 75 m/s in the part of the model covering our study region (Ward et al., 2013), which would result in a change of < 1 km in the depths of our RF arrivals.

Fig. 2 provides an example of the influence that changes to the migration velocity structure may cause in an RF CCP stack. Bins containing < 4 RFs are not plotted (appearing white) in Fig. 2 or in subsequent figures as these bins could be dominated by noise from a single RF. Fig. 2A shows RFs migrated using a half-space obtained by averaging the best fit 1-D velocity structure for the Maule region (Hicks et al., 2014); Fig. 2B shows RFs migrated using a 40 km layer over a half-space obtained by averaging the top 40 km and bottom 40 km of the Hicks et al. (2014) 1-D velocity model separately; Fig. 2C shows RFs migrated using the best fit 1-D velocity model (Hicks et al., 2014) incrementally merged with the AK135 1-D global velocity model at 80 km depth; finally, Fig. 2D shows RFs migrated using the combined Ward et al. (2013) 3-D S-wave velocity model and Hicks et al. (2014) 1-D Vp/Vs model. Fig. 2E provides a comparison between the two prominent, laterally continuous positive RF arrivals imaged by this cross-section.

In Fig. 2 and in subsequent figures, we interpret only the depth to the peak of an RF arrival (defined as the point of maximum amplitude for sharp, simple arrivals or as the mid-point of broad or complex (multi-peaked) arrivals). We do not attempt to interpret the meaning of the breadth of these arrivals as prior studies have shown that RFs are largely unable to distinguish between step-function-like, complex, and gradational discontinuities over the distance in time/depth covered by a single Gaussian pulse (Frassetto and Thybo, 2013), while these complexities do not affect the arrival time/depth of a pulse's peak (Frassetto and Thybo, 2013; Rychert et al., 2007). Given that offshore active source seismic studies at 31°S (Contreras-Reyes et al., 2014) and 38°S (Contreras-Reyes et al., 2008) have found evidence for limited hydration and/or serpentinization of the Nazca plate's upper ~2–4 km of mantle lithosphere at the trench, it is possible that the RF pulse from the subducted oceanic Moho may represent a gradational discontinuity

which would widen the RF pulse. As this hydration was attributed to outer rise faulting (Contreras-Reyes et al., 2008), it may be pervasive throughout our study region.

Examining the location of RF peaks in Fig. 2, we see that on average a slightly greater change occurs when moving from a half-space to a layer over a half-space model for both arrivals (change of ~3 km for the upper arrival and ~2 km for the lower arrival relative to the 3-D model result), possibly because this change accounts for the first order velocity structure by including the difference between the crust and mantle velocities. However, moving from a layer over half-space to a full best fit 1-D velocity model also causes a noticeable change (~2 km for both arrivals). The incorporation of the 3-D S-wave velocity model has a relatively minor average change compared to the 1-D model for the upper arrival (~1 km) and a more significant change for the lower arrival (~3 km). This appears to reflect the 3-D model's ability to account for a low velocity region immediately above the deeper RF arrival (the top of this low velocity region may be imaged by the RFs as a negative arrival above the deeper positive RF arrival). We note that the overall configuration of the prominent positive arrivals is consistent no matter which velocity model is used for migration; the 3-D model allows relatively small-scale velocity structures to be accounted for, enhancing the continuity of arrivals by helping to correct for the "stair-step" that may appear in dipping layers beneath small-scale velocity structures.

3. Results

3.1. Trench perpendicular cross-sections

Figs. 3, 4 and 5 show our trench perpendicular CCP cross-sections imaging the continental Moho and the subducted slab's oceanic Moho. Line A-A' (Fig. 3) passes through the Pichilemu anomaly, previously identified in local earthquake tomography (Hicks et al., 2014; see Fig. 3) and associated with active normal faulting at the surface (Aron et al., 2015). Beginning at $\sim\!35\,\rm km$ depth near the coast and extending to a depth of 45–50 km, a high amplitude positive RF arrival appears to lie slightly below the Slab2 surface (Hayes et al., 2018) and corresponds to the change from a Vp of 7 km/s to 8 km/s in local earthquake tomography results (Hicks et al., 2014). This feature is discontinuous below $\sim\!50\,\rm km$ depth, however a series of positive arrivals continue to approximately follow the Slab2 surface to a depth of $\sim\!80\,\rm km$. This feature likely marks the Moho of the subducting oceanic crust of the Nazca plate.

The disruption of this feature may indicate significant structural complexities in the slab in this region, unresolvable without additional data from the area. It may be significant that the disruption begins at ~50 km depth. This corresponds to the depth at which converted Ps phases indicate that the Juan de Fuca slab's curst in the Cascadia subduction zone eclogitizes (e.g. Rondenay et al., 2008). However, studies of other subduction zones indicate that slabs in other settings do not undergo eclogization until depths of ~80 to > 100 km (see Hasegawa and Nakajima, 2017 for Japan; Rondenay et al., 2008 for Alaska; Yuan et al., 2000 for central Chile). Thermal modeling suggests that the onset of eclogitization is largely linked to the thermal history of a subduction zone, with hot, recently established subduction zones or subducting young (and therefore warm) slabs leading to eclogitization at shallower depths than in colder, long established subduction zones or subducting old (and therefore cold) slabs which appear to be more controlled by the position of the volcanic arc (van Keken et al., 2011). Thermal modeling of the Maule region indicates that eclogization and associated dehydration of the Nazca slab occurs near the volcanic front at depths of ~90-100 km (Völker and Stipp, 2015). Given this, we interpret the disruption between ~50 and 80 km depth as a slab Moho that is likely structurally complex rather than an indication of significant slab crust eclogitization.

A continuous positive RF arrival at \sim 40 km depth extends beneath the Coastal Cordillera and Central Depression before deepening to

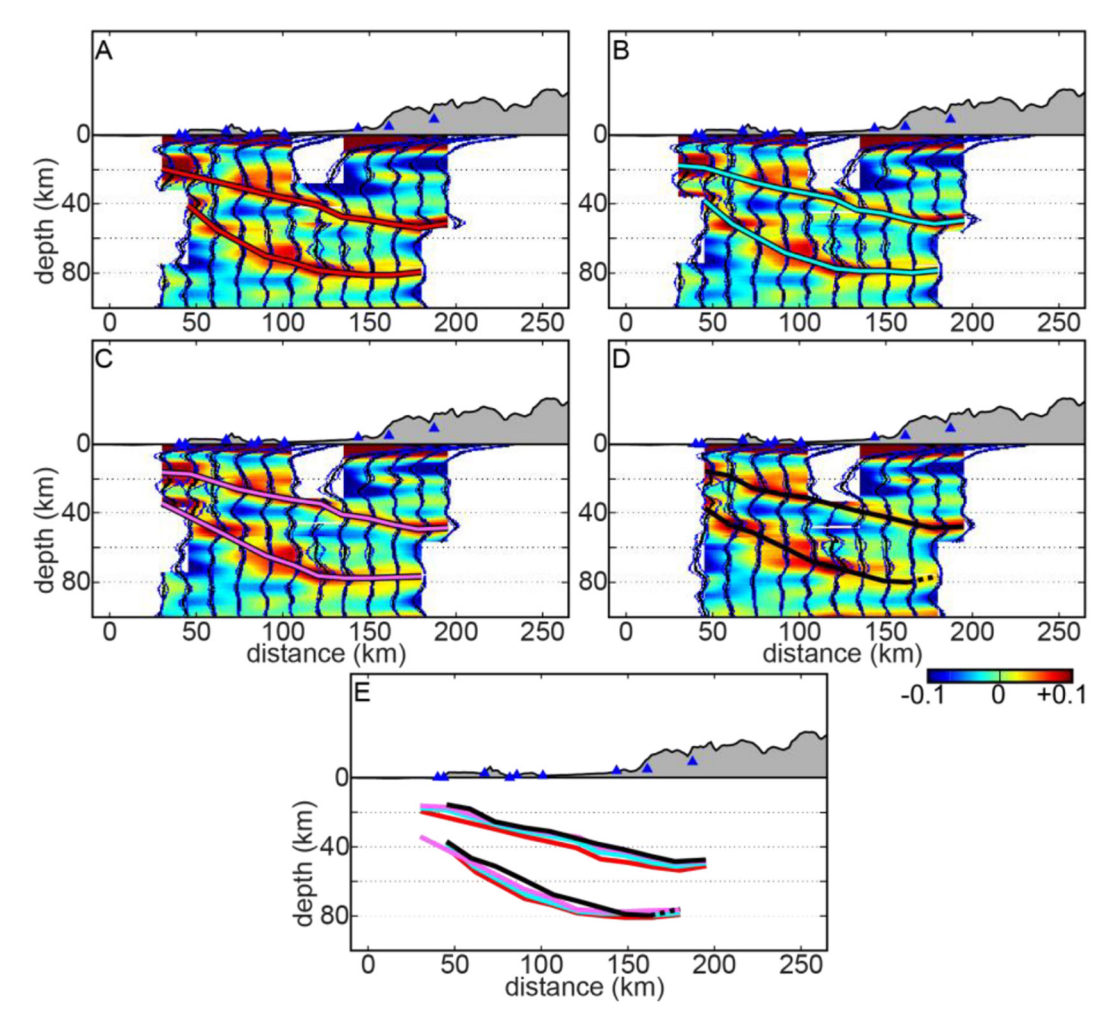


Fig. 2. Example of effects of migrating RFs with differing velocity models using the cross-section discussed in our results (see Fig. 4 for interpretation); RF color bar scale represents a unitless fraction of Ps arrival amplitudes relative to the theoretical peak amplitude of the P-direct (0-lag) arrival. A. RFs migrated using a half-space model obtained by averaging the best 1-D model obtained by Hicks et al. (2014) for the Maule region. B. RFs migrated using a layer and half-space model obtained by splitting the Hicks et al. (2014) 1-D model at 40 km depth and averaging each part separately. C. RFs migrated using the full Hicks et al. (2014) 1-D model. D. RFs migrated using our preferred 3-D S-wave velocity model for the region (Ward et al., 2013) and Hicks et al.'s (2014) 1-D Vp/Vs model for the region. E. Comparison of arrivals migrated using each velocity model (colors in E correspond to colors in A–D). Note that while all four models are broadly consistent, and unlikely to significantly alter interpretation of the relationship between the two identified arrivals, incorporation of the 3-D velocity structure may locally move a deep (> 40 km) arrival by 4–5 km. (For interpretation of the references to color in this figure legend, the reader is referred to the web version of this article.)

50–55 km beneath the Andean Cordillera. This feature marks the continental Moho and at $\sim\!140\,\mathrm{km}$ from the trench it appears to intersect the top of the subducting Nazca plate within the limits of our CCP stack's 15 km lateral resolution. These values are broadly comparable, though slightly deeper, than the $\sim\!35{-}40\,\mathrm{km}$ continental Moho depth observed by Dannowski et al. (2013) approximately 100 km southeast of our cross-section A-A'. Given Dannowski et al. (2013) stacked RFs from stations $>25\,\mathrm{km}$ apart and used a less detailed velocity model more detailed comparisons with our current study are not warranted.

The location of the intersection of the continental Moho and the slab occurs approximately below the center of the Coastal Cordillera and 30–40 km from the coastline. Near the coast, we image a positive RF arrival near 10 km depth while beneath the Central Depression we image a shallow negative RF arrival and a positive RF arrival at $\sim\!15$ km depth which appears to extend and slightly shallow beneath the Andean Cordillera. These features appear to be truncated by a region beneath the Coastal Cordillera where we find an absence of RF arrivals. This region lacking RF arrivals stretches from 25–30 km depth to <10 km depth and appears to correspond to the location of the Pichilemu anomaly (outline labelled "PA" in Fig. 3B) identified by Hicks et al. (2014). The cross-cutting relationship that this feature has with the

mid-crustal arrivals beneath the coastline and the Central Depression as well as its presence above the continental Moho arrival indicate that the Pichilemu anomaly is embedded within the continental crust. We also note that both Maule aftershock seismicity (Lange et al., 2012) and long-term seismicity, above the likely location of the megathrust, are very limited within this anomaly.

We further note the presence of a relatively broad negative RF arrival near 50– $55\,\mathrm{km}$ depth beneath, and clearly separated from, the continental Moho below the eastern most Coastal Cordillera and the Central Depression. At $> 50\,\mathrm{km}$ depth this feature is unlikely to represent the first multiple of the prominent shallow crustal negative arrival observed below the Central Depression. It is possible that this arrival represents the top of an area of relatively slow, possibly hydrated, mantle material overlying the subducting plate. We consider this possibility in conjunction with similar observations along other cross-sections below.

Line B-B' (Fig. 4) samples the region down dip of the 2010 Maule earthquake hypocenter (Duputel et al., 2012) and passes through the Cobquecura anomaly identified in a prior local earthquake tomography study (Hicks et al., 2014). A pair of gradually dipping, nearly continuous positive RF arrivals stretch from the coastline to the edge of the

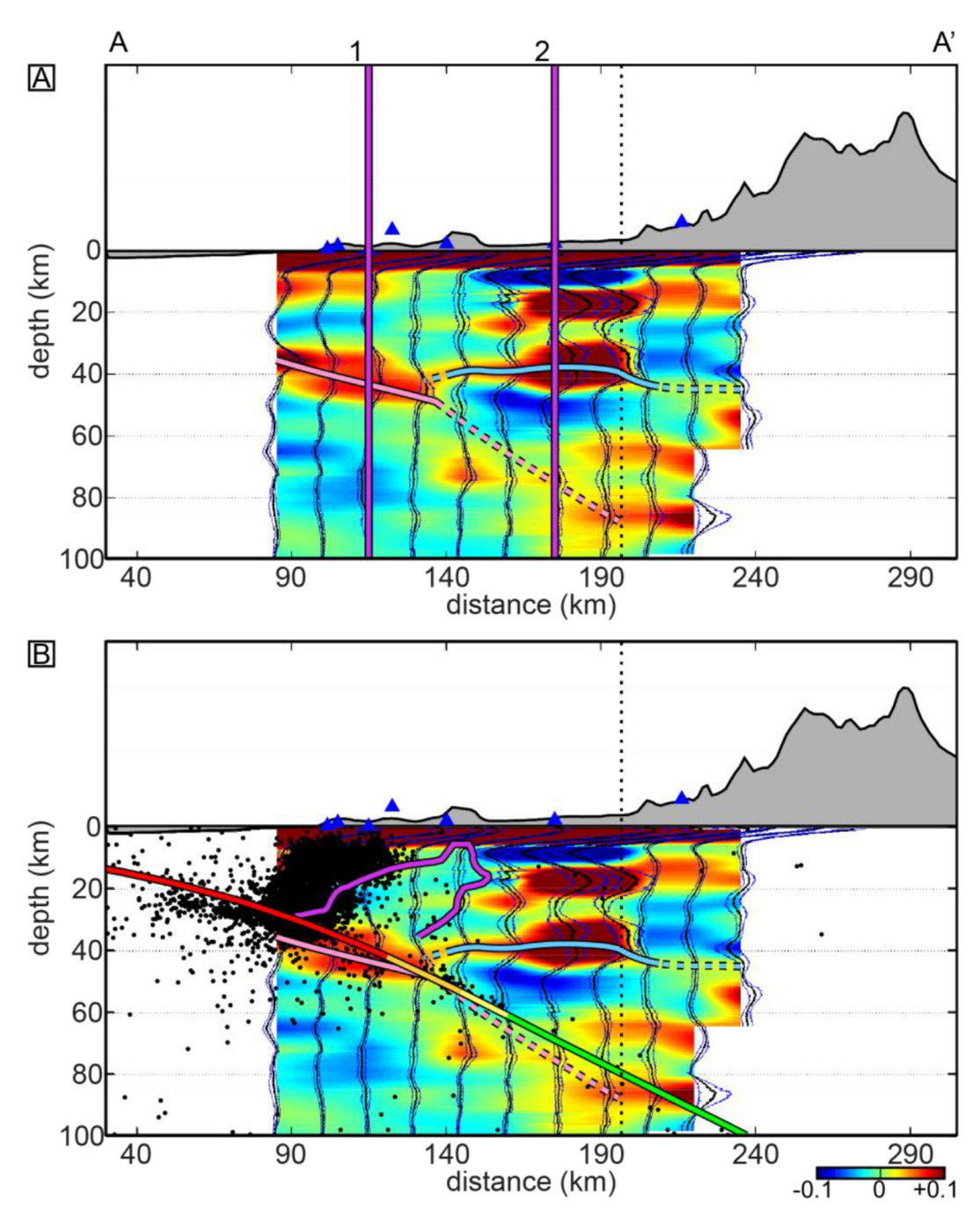


Fig. 3. Trench perpendicular RF stack cross-section A-A'; RF color bar scale represents a unitless fraction of Ps arrival amplitudes relative to the theoretical peak amplitude of the P-direct (0-lag) arrival. A. RF results and interpreted positive RF arrivals. Continental Moho (light blue line) is the relatively flat feature at ~40 km depth from 140 km to 240 km distance from the trench. The oceanic Moho (light pink line) of the subducted Nazca plate is the dipping feature from ~40 km depth at the left of image to 80 km depth at 190 km distance from the trench. Dashed where inferred. Vertical purple lines mark the intersections with trench parallel RF stacks 1-1' and 2-2' while the dashed black line is approximate predicted location of the volcanic arc high lateral thermal gradient (see Fig. 1). B. Overlay of Maule aftershock hypocenters (black dots, Lange et al., 2012). Purple line is Pichilemu high velocity anomaly defined by 7 km/s P-wave velocity contour (from Hicks et al., 2014). The Slab2 surface (Hayes et al., 2018) is colored to correspond to degrees of pre-Maule earthquake megathrust locking (Moreno et al., 2010, see also Fig. 1B) with the > 75% in red, 75% to 50% in orange, 50% to 25% in yellow, and < 25% in green. Note the rapid decrease in aftershock seismicity and the change in the Nazca plate subduction angle at the end of the strongly coupled (> 50% locking) zone. See section 3.1 for discussion. (For interpretation of the references to color in this figure legend, the reader is referred to the web version of this article.)

high Andean Cordillera. The positive arrival appearing at $\sim\!\!35\,\mathrm{km}$ depth at the coast and reaching $\sim\!\!80\,\mathrm{km}$ depth near the edge of the high Cordillera largely follows the Slab2 surface (Hayes et al., 2018) at this location, and we again interpret this feature as the oceanic Moho of the subducting plate. We interpret the shallower positive arrival to be the continental Moho. This discontinuity begins at $\sim\!\!15\,\mathrm{km}$ depth at the coast and dips gradually beneath the Coastal Cordillera and Central

Depression before flatting out at ${\sim}45\text{--}50\,\mathrm{km}$ depth beneath the Andean Cordillera.

The pronounced taper of the continental crust along this profile contrasts with the crustal structure observed in Line A-A' and indicates that here the continental crust remains well above the plate interface beneath the onshore portion of the forearc. This configuration also clearly indicates that the Cobquecura anomaly must lie within the

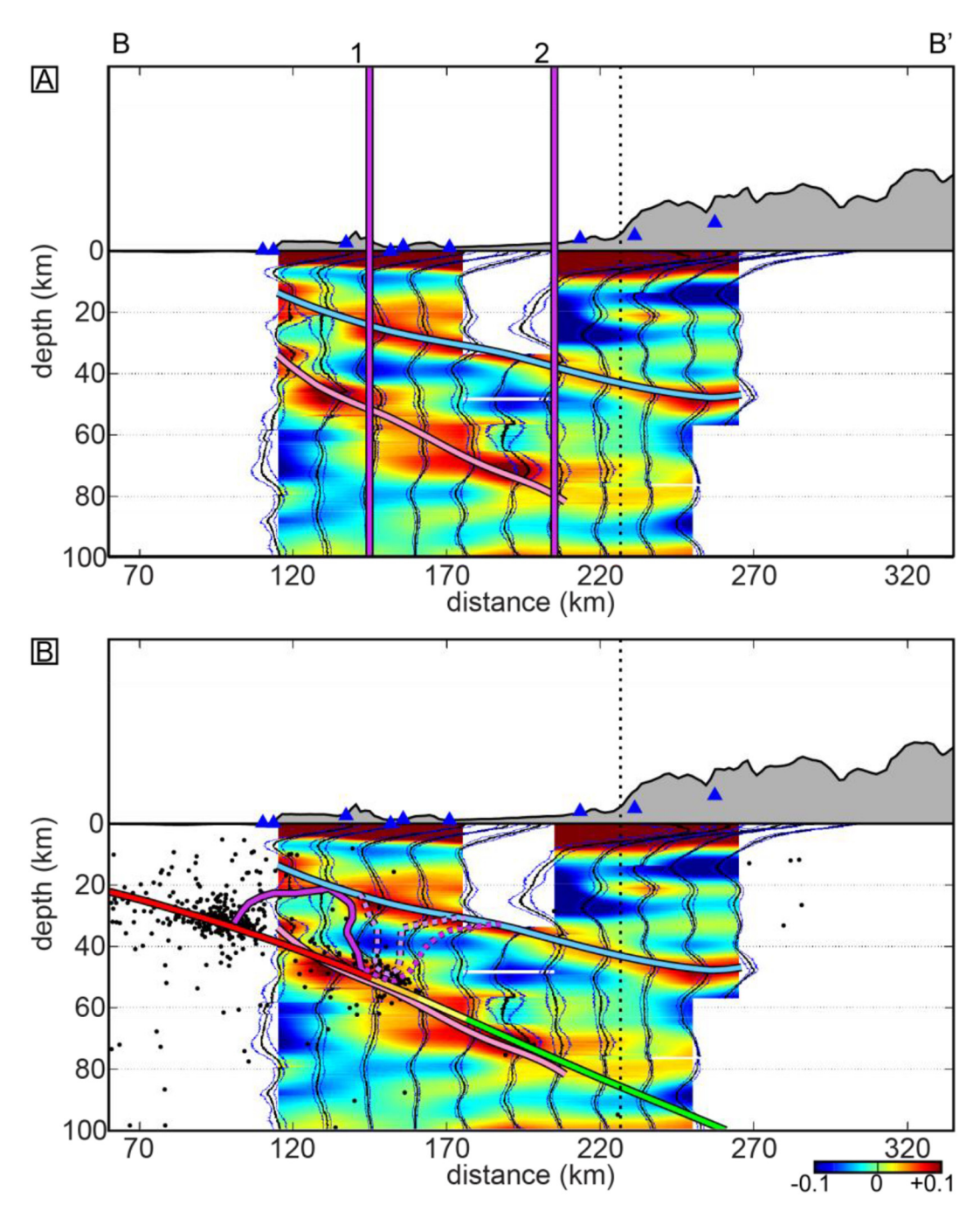


Fig. 4. Trench perpendicular RF stack cross-section B-B'; RF color bar scale represents a unitless fraction of Ps arrival amplitudes relative to the theoretical peak amplitude of the P-direct (0-lag) arrival. A. RF results and interpreted positive RF arrivals. The continental Moho (light blue line) is the upper dipping feature at \sim 15–20 km depth near 120 km lateral distance from the trench and 45 km depth at \sim 250 km from the trench. The oceanic Moho (light pink line) of the subducted Nazca plate is dipping feature from \sim 40 km depth at the left of image to 80 km depth \sim 220 km from the trench. Dashed where inferred. Vertical lines are as in Fig. 3B. Solid purple line is the Cobquecura high velocity anomaly defined by the 7.5 km/s P-wave velocity contour (from Hicks et al., 2014). Dashed dark purple line and dashed light purple line mark 7.5 km/s P-wave velocity contour respectively (from Hicks et al., 2014) that we interpret as an area of slow (partially serpentinized) mantle with a relatively abrupt boundary represented by the negative RF arrival \sim 145 km distance from trench at \sim 40 km depth. Other features as in Fig. 3B. Again, note rapid decrease in aftershock seismicity at the downdip edge of the strongly coupled (>50% locking) zone. White line near 50 km depth 190 km from trench is a small subset of bins containing <4 RFs, less than our RF hit count cutoff, which has been masked with white and should not be interpreted. See section 3.1 for discussion. (For interpretation of the references to color in this figure, the reader is referred to the web version of this article.)

forearc mantle, suggesting that this feature has a fundamentally different origin than the Pichilemu anomaly. The Cobquecura anomaly may represent a composition or hydration related mantle heterogeneity. We note that a negative RF arrival within the forearc mantle at ~40 km beneath the Coastal Cordillera and ~50 km beneath the Central Depression appears to terminate at the eastern edge of the Cobquecura anomaly, indicating a relatively abrupt lateral change in

the mantle material, supporting Hicks et al.'s (2014) interpretation of the Cobquecura anomaly as a mantle heterogeneity.

Line C-C' (Fig. 5) passes through the Arauco Peninsula, a feature consistently associated with the southern limit of slip during the 2010 Maule earthquake (Delouis et la., 2010; Lorito et al., 2011; Moreno et al., 2012; Yue et al., 2014) and identified as a possible long-term impediment to the rupture of large megathrust earthquakes (Dura et al.,

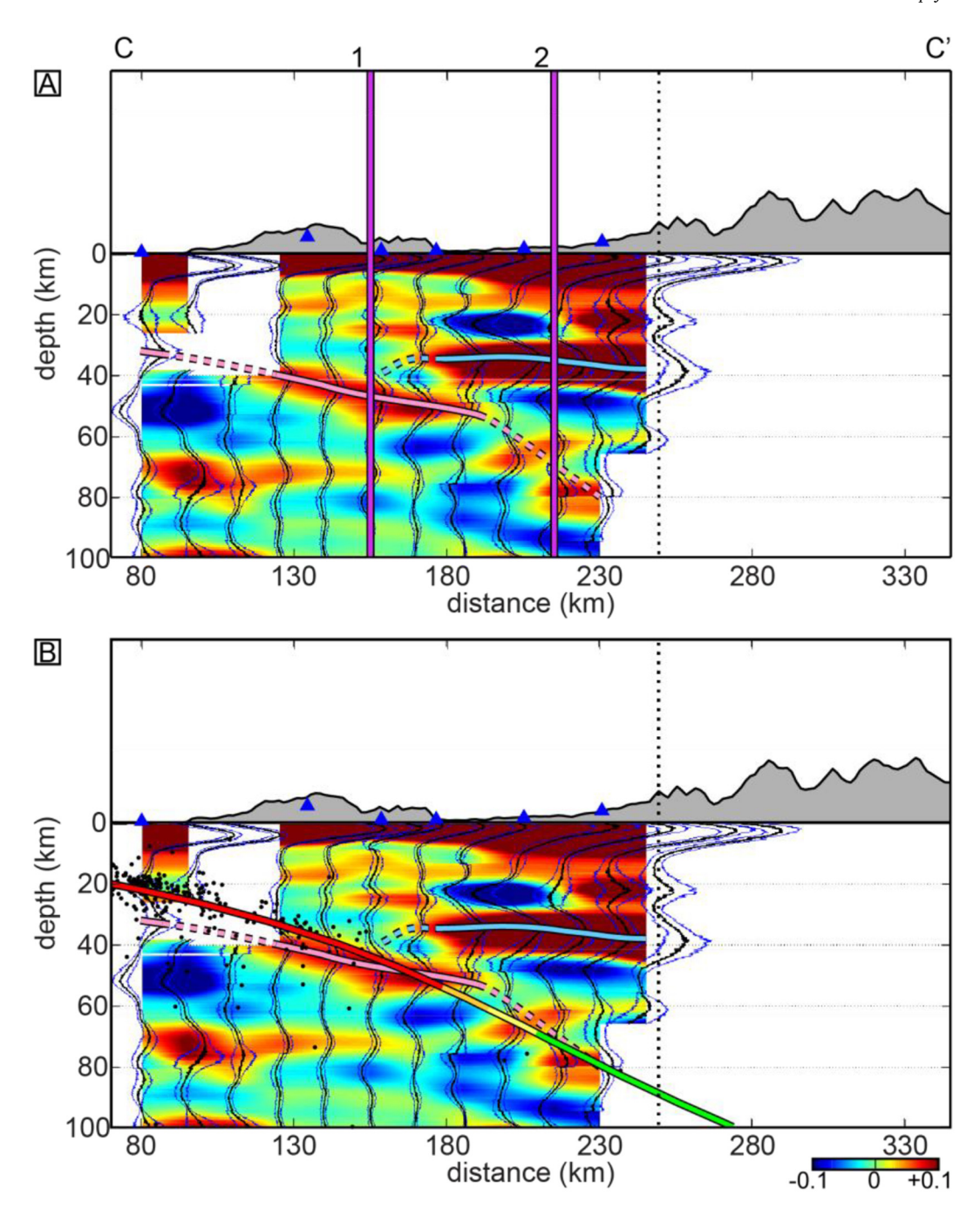


Fig. 5. Trench perpendicular RF stack cross-section C-C'; RF color bar scale represents a unitless fraction of Ps arrival amplitudes relative to the theoretical peak amplitude of the P-direct (0-lag) arrival. A. RF results and interpreted positive RF arrivals. The continental Moho (light blue line) is the flat and very high amplitude positive feature at \sim 35–40 km depth near 180 km from the trench to \sim 240 km from the trench. The oceanic Moho (light pink line) of the subducted Nazca plate is the dipping feature from \sim 20 km depth at left of image to 80 km depth at 230 km distance from the trench. Dashed where inferred. Vertical lines are as in Fig. 3A. B. Cross-section C-C' with overlay of Maule aftershock hypocenters (black dots, Lange et al., 2012). Other features as in Fig. 3B. See section 3.1 for discussion. (For interpretation of the references to color in this figure legend, the reader is referred to the web version of this article.)

2017). As in the above cross-sections, we associate the positive RF arrival immediately below the Slab2 surface with the Moho of the subducted oceanic crust. This feature appears at $\sim 30\,\mathrm{km}$ depth at the coast and dips eastward beneath the Coastal Cordillera to a depth of 50–55 km before the RF arrival becomes discontinuous at a depth of 65–80 km beneath the Central Depression, Under the Central Depression, the continental Moho appears as a very prominent high amplitude arrival that dips gradually from $\sim 35\,\mathrm{km}$ depth at the eastern edge of the Coastal Cordillera to $\sim 40\,\mathrm{km}$ depth at the western edge of the high Andean Cordillera. We observe no clear arrival for the continental Moho beneath the Coastal Cordillera, suggesting the continental crust

and the subducting oceanic crust are in contact at this location. While the relatively weak positive arrivals beneath the Coastal Cordillera at \sim 20 to \sim 25–30 km depth could represent the continental Moho, reported P-wave velocities of < 7.0–7.5 km/s at these depths in this location (Hicks et al., 2014) are not consistent with mantle material. In addition, geophysical results centered on 38.2°S, \sim 60 km south of the location of C-C', show a very similar pattern of layering at these depths (Groß et al., 2008) associated with < 7.0–7.5 km/s Vp and < 1.72 Vp/Vs (Haberland et al., 2009) interpreted as continental crustal material extending to the top of the subducting slab beneath the Coastal Cordillera (Groß et al., 2008; Haberland et al., 2009). Clear layering is

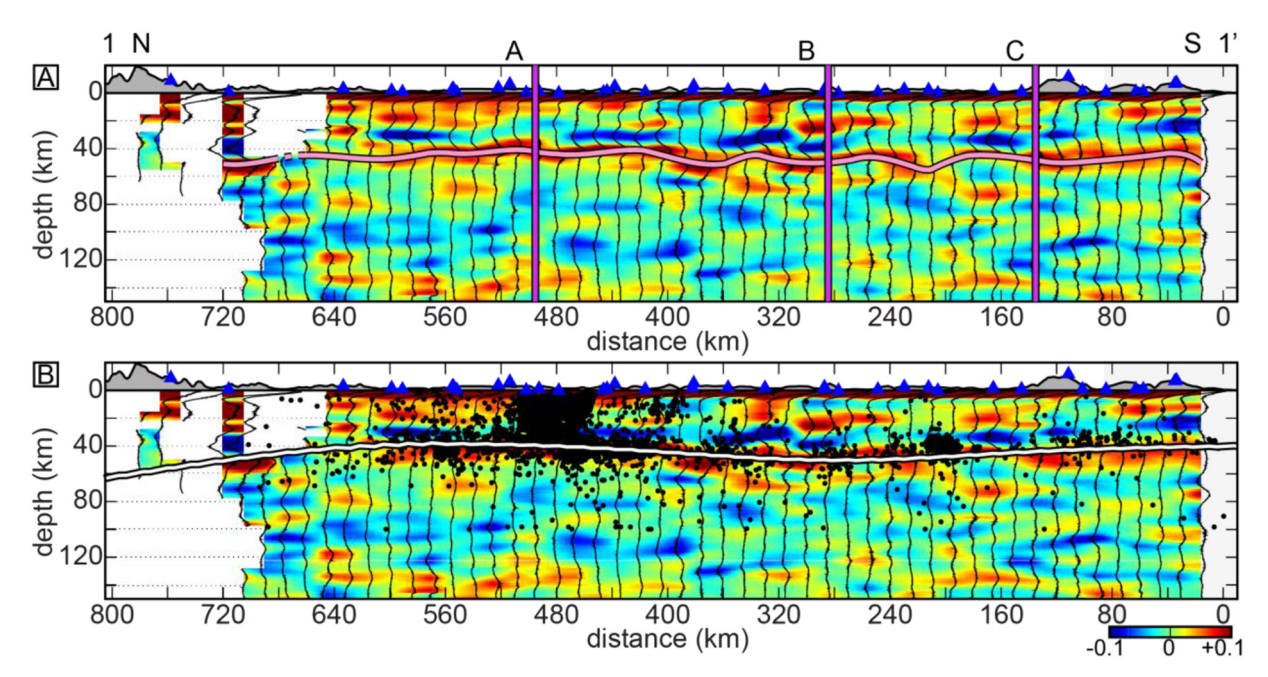


Fig. 6. Trench parallel cross-section 1-1', approximately following the down dip limit of strong plate locking (see Fig. 1); RF color bar scale represents a unitless fraction of Ps arrival amplitudes relative to the theoretical peak amplitude of the P-direct (0-lag) arrival. A. The forearc continental Moho is extremely heterogeneous at this scale and we do not attempt to trace it. The Moho of the subducted Nazca plate's oceanic crust (light pink line) can be followed laterally throughout most of study region and lies near ~40 km depth. Vertical purple lines mark intersections with trench perpendicular cross-sections A-A', B-B', and C-C'. B. Features as in Fig. 3. Note that Slab2 (white line) exhibits greater long-wavelength variation in depth than our RF slab Moho or aftershock seismicity. See section 3.2 for discussion. (For interpretation of the references to color in this figure legend, the reader is referred to the web version of this article.)

present in the Coastal Cordilleran continental crust, and the lower layer near $\sim\!25\,\mathrm{km}$ depth may truncate westward against the plate interface. Structures within the Central Depression's continental crust may be obscured by basin-induced reverberations, making it difficult to interpret the eastward continuation of features within the Coastal Cordilleran crust.

As in Lines A-A' and B-B', we note that a negative RF arrival appears within the forearc mantle beneath the continental Moho of the Central Depression near ~50 km depth. These arrivals may mark the top of features analogous to the localized low velocity features observed by Haberland et al. (2009) near 38°S and interpreted as possible pockets of hydrated, serpentinized forearc mantle. However, our observed continental Moho arrivals along all three lines are distinct positive RF velocity contrasts and we agree with Dannowski et al. (2013) that this requires that the mantle immediately below the forearc's crust remains seismically fast and unserpentinized.

3.2. Trench parallel cross-sections

Line 1-1' (Fig. 6) and Line 2-2' (Fig. 7) approximately parallel the trench (presumably approximating the strike of the megathrust) and sample, respectively, the downdip edge of significant pre-2010 Maule earthquake plate coupling (Fig. 1; Moreno et al., 2010) and 60 km further inboard. This distance insures no overlap in the RFs stacked to calculate the two cross-sections, highlighting inboard differences in the geometry of the subducting oceanic plate's Moho. Along Line 1-1' the subducted plate's oceanic Moho appears consistently at a depth of ~45–50 km while along 2-2' this feature appears at a depth of ~70–80 km with noticeable variations in depth along the length of the cross-section. Potential variation in slab depth and trench parallel dip have been invoked to explain coastal uplift processes in the Maule region (Melnick et al., 2009; Jara-Muñoz et al., 2015) and a better understanding of slab depth variations offers an opportunity to investigate these proposed models.

To better understand this variation, we first plotted a set of fourteen trench parallel RF profiles in our study region and identified the slab oceanic Moho along each profile. In order to compare slab Moho depths between profiles, we then calculated the mean depth of the slab Moho for each profile, subtracted this from the corresponding slab Moho picks, and finally calculated the average deviation for the slab Moho picks along each profile (see Table 1 for maximum, minimum and average deviation along each profile as well as the number of slab Moho observations recorded along the profiles; see Supplemental Table 1 for latitude, longitude, and depth of each slab Moho observation). The average deviation for each profile can be interpreted as a measure of the degree of trench parallel upwarping or downwarping that has occurred in the slab. We exclude profiles 1-3 and 13-14 from further consideration as they sample less than half of our study region. The remaining profiles can be divided into two distinct groups: profiles 4-6 with average deviations of 2 km to 3 km and profiles 7-12 with average deviations between 5 km and 8 km. The rapid transition between these two groups falls between profiles 6 and 7, approximately at the switch from high (> 75%, largely sampled by profile 6) to low (< 75%, largely sampled by profile 7) coupling between the overriding and subducting plates (Moreno et al., 2010). See section 4.1.2 for further discussion of this variation and its implications for coastal uplift models of the region.

4. Discussion

The observations we present in section 3 have a number of implications for the understanding of forearc seismicity and the long-term (100 kyr to > 1 Myrs) evolution of forearcs. In section 4.1, we consider different aspects of the Chilean forearc between 32°S and 39°S separately before considering how these aspects may be tied to large-scale, inherited structures within a forearc's upper plate in sections 4.2 and 4.3.

4.1. The continental Moho and seismogenic megathrust

The precise relationship between the depth at which the continental Moho of an overriding plate intersects the subduction interface and the

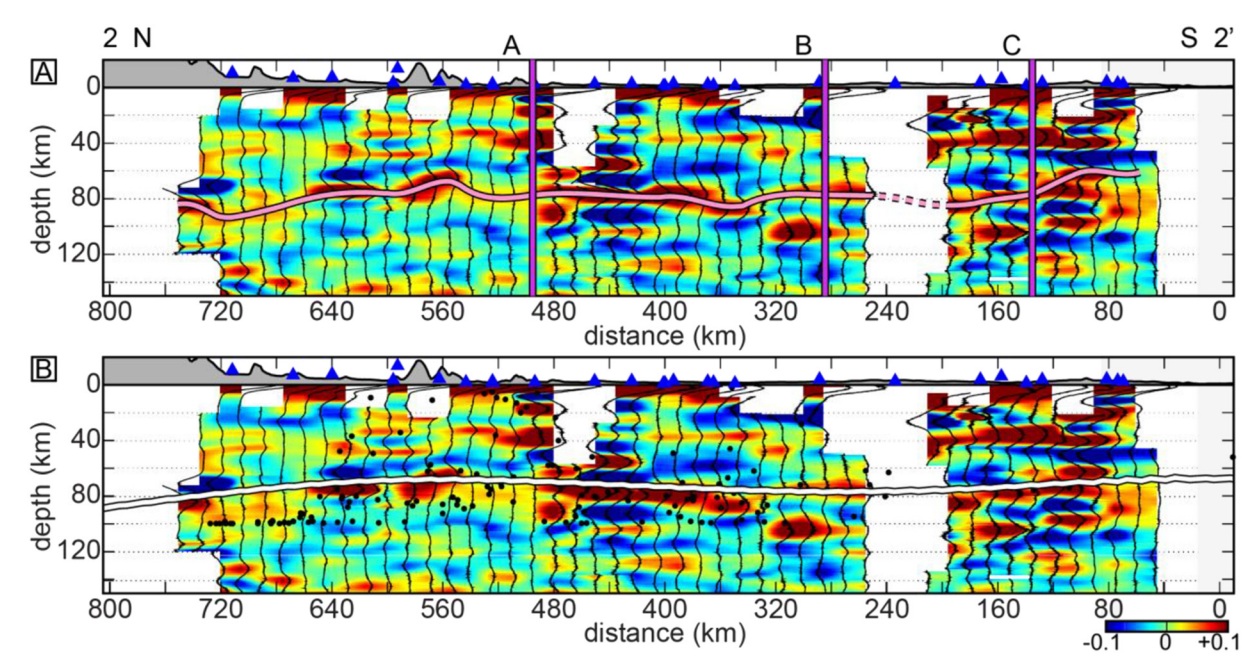


Fig. 7. Trench parallel cross-section 2-2', beyond the down dip limit of strong interplate locking; RF color bar scale represents a unitless fraction of Ps arrival amplitudes relative to the theoretical peak amplitude of the P-direct (0-lag) arrival. A. The forearc continental Moho is again extremely heterogeneous at this scale and we do not attempt to trace it. The Moho of the subducted Nazca plate's oceanic crust (light pink line) can be followed laterally throughout much of study region, and lies near ~80 km to ~100 km depth. Vertical purple lines mark intersections with trench perpendicular cross-sections A-A', B-B', and C-C'. B. Features as in Fig. 6. Note that in contrast to cross-section 1-1' (Fig. 6) the variation in depth of Slab2 (white line) is similar to our RF slab Moho, though smoother; at this depth, aftershock seismicity represents intermediate depth earthquakes and may represent events within the subducted slab's crust or mantle rather than events on the plate interface (e.g. Ferrand et al., 2017; Wang et al., 2017). See section 3.2 for discussion. (For interpretation of the references to color in this figure legend, the reader is referred to the web version of this article.)

Table 1
Vertical deviations in slab Moho depth along trench parallel lines relative to average depth along each line.

Line number	Data points (out of 54)	Minimum deviation (km)	Maximum deviation (km)	Average deviation (km)
1	4	-1.2	1.0	0.62
2	6	-1.1	1.6	0.97
3	20	-4.0	6.2	2.52
4	36	-7.4	5.8	2.66
5	46	-7.2	8.0	2.6
6	46	-6.3	10.6	3.14
7	41	-9.6	16.3	5.75
8	38	-13.8	15.4	6.67
9	31	-11.8	13.9	6.23
10	42	-16.9	18.3	5.48
11	42	-12.2	19.1	6.56
12	32	-11.6	17	6.66
13	20	-12.7	14.5	7.98
14	5	-2.7	3.8	2.02

depth to the bottom of the seismogenic megathrust has been a point of interest in understanding great earthquakes (e.g. Wang and Tréhu, 2016 and references therein) and, within the Andean forearc, in understanding the processes driving large-scale uplift of the coast over many earthquake cycles (e.g. Melnick, 2016). As shown in our results (Figs. 3, 4, and 5), the relationship between the continental Moho and the megathrust throughout the region ruptured by the $8.8~\mathrm{M}_W$ 2010 Maule earthquake and subsequent aftershocks varies significantly from north to south. Yet the down-dip rupture limit of the 2010 Maule earthquake appears to be at ~40 km depth along the entire length of the rupture. This presents a significant challenge (well beyond our abilities to resolve in the present study) to any model proposing to explain earthquake (see Wang and Tréhu, 2016; Gao and Wang, 2017 for review of these models) or coastal uplift processes (e.g. Melnick, 2016) on the basis of the intersection of the continental Moho and

seismogenic megathrust interface. To better visualize the relationship between the continental Moho-slab intersection and prior geological and geophysical observations of the Maule region, we have plotted the trenchward and arcward constraints on its position as determined by a set of thirty-nine trench perpendicular RF cross-sections (Fig. 8A). We can constrain the intersection's location, at best, to a swath with the width of one CCP-stack bin (~15 km).

We recognize three distinct along-strike zones (Fig. 8A) with characteristics broadly similar to the three trench parallel cross-sections presented above: a northern zone between ~33.5°S and ~35.5°S similar to Line A-A' (see Fig. 3), though typically lacking the feature we associate with the Pichilemu anomaly; a central zone between ~35.5°S and ~36.5°S similar to Line B-B' (see Fig. 4); and, following a structurally complex transition, a southern zone between 37.25°S to ~38. 5°S similar to Line C-C' (see Fig. 5). This segmentation appears to define an anomalous central segment, bounded by the Cortaderas Lineament and Bio-Bio Fault, where the continental Moho is warped upward above the Cobquecura anomaly and potentially above the location of the 2010 Maule earthquake hypocenter (Fig. 8B).

4.1.1. Continental Moho and earthquake processes

Wang and Tréhu (2016) classify existing definitions of the seismogenic portion of a megathrust into four categories: rate-state frictional properties; large earthquake ruptures; interseismic locking; and small-to-medium sized earthquake distribution. The latter three of these can be established in our study area based on existing geophysical observations of the Maule region. The region of significant (~5 m) coseismic slip caused by the 2010 Maule earthquake (Yue et al., 2014) is shown in Fig. 8B in blue. The extents of 50% and 25% pre-2010 Maule earthquake interseismic locking (Moreno et al., 2010) are shown in Fig. 8B in orange and yellow respectively. We have not plotted aftershock seismicity for the 2010 Maule earthquake in Fig. 8B for clarity, however as shown in our RF profiles (Figs. 3B, 4B, 5B) the limit of significant aftershock seismicity generally corresponds to the downdip

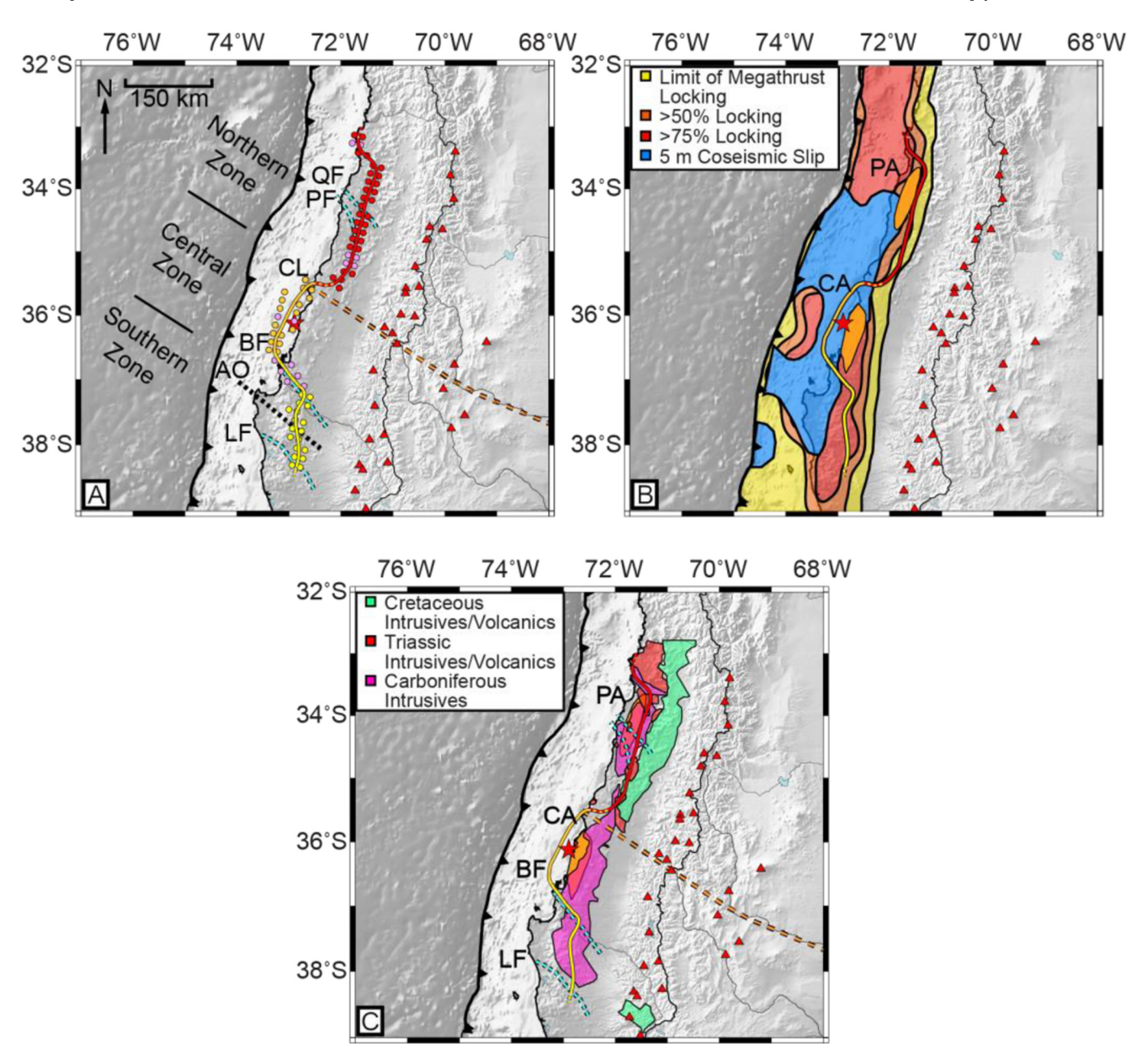


Fig. 8. Relationship of northern, central, and southern zones of the Maule forearc to other geophysical and geological features. A. Map of RF constrain points used to determine the approximate (\sim 15 km to \sim 30 km uncertainty given RF bin size) position of the megathrust—continental Moho intersection. Southern zone in yellow (characterized by \sim 35–40 km thick crust and an intersection far from the coast); central zone in orange (characterized by < 30 km thick crust and an intersection at the coast or slightly offshore); northern zone in red (characterized by \sim 35–50 km thick crust and an intersection relatively far from the coast). Purple points mark RF profiles sampling complex crustal structure or with insufficient coverage near the coast to determine the location of the intersection; point of intersection is inferred to smoothly transition between neighboring profiles with clearer observed megathrust—continental Moho intersection locations. Dashed cyan line BF is the Bio-Bio Fault; dashed cyan line LF is the Lanalhue Fault. Other features are the same as in Fig. 1A.

B. Intersection as in A, but showing slip (modified from Yue et al., 2014) and plate interface locking degree (modified form Moreno et al., 2010) and Hicks et al.'s (2014) Cobquecura (orange feature labelled CA) and Pichilemu (orange feature labelled PA) high P-wave velocity anomalies.

C. Intersection as in A, but showing high velocity anomalies from B and with simplified surface exposure of intrusive bodies and volcanics (modified from compilation in Hicks et al., 2014) overlain. Note that the Cobquecura anomaly (CA) lies below Carboniferous batholith in only the region north of the Bio-Bio Fault (BF) despite the batholith continuing south to Lanalhue Fault (LF). Note that Pichilemu anomaly (PA) is obscured by overlying intrusive body exposures, refer to B for clarification of location. (For interpretation of the references to color in this figure legend, the reader is referred to the web version of this article.)

limit of 50% interseismic locking. In the northern and southern zones, these measures of the seismogenic section of the megathrust approximately match the position of the megathrust—continental Moho interface. In the central zone, and possibly in the transitional area between the central and southern zones, the seismogenic portion of the megathrust extends well downdip of the megathrust—continental Moho interface.

Models of subduction zone megathrusts (e.g. Kato et al., 2010; Peng and Gomberg, 2010; Gao and Wang, 2017) generally agree in placing the limit of the seismogenic zone at or above the intersection of the megathrust and continental Moho while disagreeing on the precise relationship between the intersection and other megathrust processes. The northern and southern zones of the Maule region appear to agree with these models, however the central zone is a clear exception. This

may in part be due to the unusually attenuated continental crust in this location (see Fig. 4) which tapers to $< 20 \, \mathrm{km}$ thickness at the coast, allowing forearc mantle material to occupy depths more typically occupied by continental crust in continental active margin settings. This central segment also contains both the Cobquecura anomaly as determined by seismic tomography (Hicks et al., 2014) and the hypocenter for the 2010 earthquake. It appears that the 2010 earthquake initiated at or near the intersection of the continental Moho and the top of the slab updip of the Cobquecura anomaly (Fig. 8B).

This unusually shallow forearc mantle may help to explain the lack of correspondence between the megathrust-continental Moho interface and the bottom of the seismogenic zone. Hyndman and Wang (1993) have shown that a relatively simple model is capable of describing the stick-slip frictional behavior necessary to induce earthquakes and the transition to stable sliding behavior at temperatures greater than ~350 °C. Subsequent work indicates that this may be a minimum temperature for the transition to stable sliding behavior and that seismogenic stick-slip behavior may continue up to 450 °C (Hyndman et al., 1995) or even 600 °C for specific dry rock types (Mitchell et al., 2015). Numerical modeling of the Chilean forearc in the Maule area (Völker and Stipp, 2015) indicates that the megathrust is unlikely to reach the 350 °C minimum temperature until depths of 35-40 km. This range of depths is consistent with the approximate depth to the megathrust-continental Moho interface in the northern and southern zones in the Maule region (Figs. 3 and 5). But the seismogenic interface extends significantly below the depth of the continental Moho in the central zone (Fig. 4). In addition, 35-40 km is the approximate depth at which interseismic locking and aftershock seismicity begin to decreases in the central zone (Fig. 4). This suggests that the discordance between the megathrust—continental Moho interface and the downdip limit of the seismogenic zone in the Maule region's central zone is a result of the forearc Moho in this location being unusually shallow and therefore ~50-100 °C colder than would otherwise be the case.

Our observations in Maule region are similar to the model proposed by Gao and Wang (2017) for subduction along the Japan Trench where the subduction zone is relatively cold, however in the Maule region it is the varying upper plate crustal thickness that plays a key role rather than the overall temperature of the subduction zone. A relatively shallow continental Moho at the coast (< 30 km depth) and intersections with the megathrust offshore have also been observed locally along parts of the forearc adjacent to the Japan Trench (e.g. Hasegawa et al., 1994; Nakajima et al., 2002). This suggests that even along the Japan Trench variations in the upper plate's crustal thickness may be a significant factor in determining the relationship between the forearc Moho, the megathrust seismogenic zone, and the subduction zone's thermal structure.

The structural differences at depth between the northern, central, and southern zones may also help to explain rupture behavior during the February 2010 Maule earthquake. While the absolute rupture velocities reported by Kiser and Ishii (2011) and by Huang et al. (2017) for the earthquake differ, both studies found that rupture propagated noticeably faster north of $\sim 35.5^{\circ} \text{S}$ to 36°S than south of these latitudes, broadly corresponding with our northern and central zones, respectively. Kiser and Ishii's (2011) more detailed model for the propagation of the 2010 Maule earthquake's rupture shows a rapid change or jump in rupture velocity, possibly indicating a localized lack of coseismic slip, as it moved northwest from 35.5°S to 35°S , again corresponding to the relatively sharp boundary between our northern and central zones.

4.1.2. Continental Moho and coastal uplift processes

The correspondence between the boundary of our central and southern zones and the Bio-Bio Fault (see Fig. 8A and C) is interesting as this fault marks the northern boundary of forearc uplift associated with Arauco Peninsula and Arauco Orocline (Jara-Muñoz et al., 2015). The arcward step in the megathrust—continental Moho interface that

begins at this fault continues north-south along a trend of \sim 73°W until reaching the Lanalhue Fault. This large pre-Mesozoic left-lateral strikeslip fault marks a major change in forearc structure where Permian-Carboniferous granitoids are juxtaposed against Carboniferous-to-Triassic accretionary wedge materials (Glodny et al., 2006; Glodny et al., 2008b). Uplift of the forearc between the Bio-Bio and Lanalhue Faults has been constrained by the presence of Pliocene marine sedimentary rocks exposed on part of the uplifted peninsula (Mordojovich, 1981). Glodny et al. (2008a) used apatite fission track thermal modeling to determine a rate of rock uplift of > 0.2 mm/yr (> 0.2 km/Myr) for the Coastal Cordillera between these two faults. Along the coast, Jara-Muñoz et al. (2015) dated uplifted Pleistocene marine terraces and found an uplift rate of 1.59 m/kyr (1.59 km/Myr) for the peninsula. Both studies indicate that uplift of the Arauco Peninsula and adjacent Coastal Cordillera is a Pleistocene to Holocene process.

A number of mechanisms have been called upon to explain the uplift of the peninsula. Melnick et al. (2009) suggested that uplift of the Arauco Peninsula has been driven by collision of a northward moving forearc sliver with a stronger segment of the forearc since ~4 Ma. This stronger segment could be caused by either an abrupt transition in basement rocks across the Lanalhue Fault or by a length of relatively shallower slab subducting beneath the peninsula (Melnick et al., 2009). Jara-Muñoz et al. (2015) used a gravity derived model of the depth to the subducting Nazca plate to refine the shallow slab model and suggested that the Arauco Peninsula lies above a segment of slab that is shallower than the region to the north. This shallow segment of slab could increase the amount of permanent deformation in the upper plate during large earthquakes, leading to the peninsula's uplift (Jara-Muñoz et al., 2015).

In contrast to these structural models, Saillard et al. (2017) suggested that differences in the megathrust's rheology occur beneath peninsulas along the South American margin, including the Arauco Peninsula. Beneath these peninsulas, the megathrust tends to creep or slide aseismically, leading to permanent deformation capable of driving forearc uplift. In this model, uplift of peninsulas over ~100 kyr to ~1 Myr time scales reflects persistent differences in the frictional properties of the megathrust (Saillard et al., 2017). Variation in megathrust properties is also an important feature of Melnick's (2016) model which links coastal uplift to the position of interplate earthquakes relative to the continental Moho. Relatively deep, large megathrust earthquakes occurring near the Moho act to uplift the coastline while shallower large events (like the 2010 Maule earthquake) lead to coastal subsidence (Melnick, 2016).

While our present study cannot address all aspects of these models, our observations of the geometries of the subducting Nazca slab and of the megathrust—continental Moho intersection are useful in evaluating parts of these models. We find that the depth to the subducted Nazca plate's Moho is relatively flat along trench parallel RF profiles. We find only minor variation (no $> \pm 10\,\mathrm{km}$ and generally $< \pm 8\,\mathrm{km}$ from a profile average) along profiles sampling the plate interface to the approximate down dip limit of plate coupling (see Table 1). These minor variations do not appear to correspond to the Arauco Peninsula. This argues against the plate interface acting to strengthen the forearc beneath the peninsula or otherwise promoting uplift of this part of the forearc as required for Melnick et al.'s (2009) and Jara-Muoz et al.'s (2015) models.

The location of the megathrust—continental Moho interface also suggests that the 2010 Maule earthquake, while nucleating at a shallow depth, may have occurred at or very near the depth at which the continental Moho intersects the megathrust (see Fig. 8). In Melnick's (2016) model an earthquake nucleating near the depth of the continental Moho is predicted to be associated with uplift. In the 2010 Maule earthquake the coastline near the hypocenter experienced subsidence (Farías et al., 2010b). This suggests that Melnick's (2016) model may need to incorporate additional factors beyond the location of the megathrust—continental Moho intersection, possibly including a more

variable relationship between the crustal and thermal structures of the megathrust. Melnick's (2016) model assumes a correspondence between the depth to the base of the megathrust's locked zone and the continental Moho. As we discussed in the previous section, the depth to the base of the locked megathrust may correspond to a thermally controlled change from brittle to ductile behavior and this may not be coincident with the depth of the continental Moho. In the area around the hypocenter of the 2010 Maule earthquake, the depth of the continental Moho is significantly shallower than the base of the locked megathrust and the continental crust would not likely experience the style of deformation called for by Melnick's (2016) model of coastal uplift.

Finally, both the increase in crustal thickness south of the Bio-Bio Fault and the corresponding westward jump in the megathrust-continental Moho intersection have implications for models calling for abrupt changes in the forearc basement across the faults bounding the Arauco Peninsula (Melnick et al., 2009) or for a difference in plate interface properties beneath the peninsula (Saillard et al., 2017). The high velocity, high density mantle of the Cobquecura anomaly (Hicks et al., 2014) lies immediately north of the Bio-Bio Fault at a shallow depth, and this could affect both the forearc basement and the plate interface's frictional properties. This material may be more resistant to deformation than the forearc crust that lies at a comparable depth immediately to its south. If so, it would act as a strong backstop for the forearc sliver hypothesized to be moving northward towards the Arauco Peninsula from the south (Melnick et al., 2009). If the Lanalhue Fault represented the backstop for this forearc sliver, compression should occur to the south of the fault. Instead, observed uplift largely occurs north of the Lanalhue Fault. This places the uplift just south of the Bio-Bio Fault. Combined with the observation that significant uplift does not extend north of the Bio-Bio Fault (Jara-Muñoz et al., 2015), this suggest that the Cobquecura anomaly north of the Bio-Bio Fault serves as a backstop, leading to deformation within the relatively weak material beneath the Arauco Peninsula as the forearc sliver south of the peninsula moves northward.

Beneath the Arauco Peninsula and neighboring Coastal Cordillera the intersection between the continental Moho and subducting Nazca plate occurs at a greater depth and comparatively greater distance inboard than north of the Bio-Bio Fault. The presence of continental crust for a longer down-dip length of the plate interface beneath the Arauco Peninsula likely leads to a difference in megathrust frictional properties relative to the region north of the Bio-Bio Fault. This difference would be consistent with Saillard et al.'s (2017) model. Alternately, the lower ~10–20 km of this thicker crust may be underplated trench sediments or off-scraped forearc rock as suggested by Haberland et al. (2009). If so, we note that the pre-underplating crust beneath the Arauco Peninsula may have been only 20–30 km thick. This is comparable to the thin crust we observe in our central zone north of the Bio-Bio Fault. We consider this possibility, as well as why underplating may be localized beneath the Arauco Peninsula and adjacent Coastal Cordillera, in the next section

An additional area of coastal uplift also occurs in the Maule rupture region without an associated major peninsula. Jara-Muoz et al.'s (2015) examination of marine terrace uplift identifies the area between the Pichilemu and Topocalma Faults as an area of significant (~1.35 m/kyr or 1.35 km/Myr) coastal uplift. This is attributed to a combination of basal accretion, forearc sliver motion, or a shallow plate interface (Jara-Muñoz et al., 2015). Our observations allow us to investigate the third proposed mechanism. As noted above, we find that the depth to the Nazca slab along the plate interface shows no significant trench parallel change throughout the Maule region. This indicates that there is no significant difference in the subducting plate geometry around Pichilemu and that a combination of basal accretion and/or forearc sliver motion as called for in Jara-Muoz et al.'s (2015) uplift model are likely to be more important for the area.

4.2. Forearc mantle heterogeneity: a key to long-term structure preservation?

One of the most striking features we observe in the Maule region is the Cobquecura anomaly (Hicks et al., 2014; see Figs. 4 and 8B, C) and the associated shift in the position of the megathrust-continental Moho interface's relationship relative to the other elements of the subduction zone. The Cobquecura anomaly is associated with P-wave seismic velocities up to $\sim 8.0 \, \text{km/s}$ and a Vp/Vs ratio of ~ 1.81 and lies immediately up dip of an area of low P-wave velocity (< 7.25 km/s, dashed purple line in Fig. 4B) and high Vp/Vs (> 1.81) material (Hicks et al., 2014). This configuration is consistent with our RF results for the central zone (Fig. 4) which finds that the Cobquecura anomaly's down dip limit truncates at a relatively low velocity layer of mantle material immediately above the slab. The seismic velocities of the anomaly led Hicks et al. (2014) to interpret the Cobquecura anomaly as unserpentinized mantle, and while we agree with this interpretation we note that this strong, unserpentinized block of mantle lies directly adjacent to an area with seismic velocities more characteristic of a highly serpentinized (> 40% by volume antigorite (Abers and Hacker, 2016) given the values reported by Hicks et al. (2014)) mantle (see Fig. 4B).

The juxtaposition of these materials over a short (~15 km) lateral distance suggests that the composition of the Cobquecura anomaly may differ from typical mantle peridotite. In continental forearc settings, serpentinization results from the hydration of olivine within mantle rocks to form antigorite (Reynard, 2013), and peridotite provides a ready source of olivine for this process. If the Cobquecura anomaly is dominantly peridotite, it is difficult to explain why it would remain unserpentinized while neighboring mantle materials show evidence for significant serpentinization. Continuous subduction in this region began at ~180 Ma (Ramos and Kay, 2006), which means that the forearc mantle in this location should be \sim 20% hydrated (Abers et al., 2017) and at least partially serpentinized. A non-peridotite composition may explain this discrepancy. Ultramafic cumulates like garnet pyroxenite (or "arclogite") are largely free of olivine (Ducea, 2002; Lee and Anderson, 2015), preventing significant serpentinization, and possess high P-wave (~7.9 to 8.0 km/s) and relatively high Vp/Vs (1.79-1.80) values (Frassetto et al., 2011). The production of garnet pyroxenite is associated with continental arc volcanism and the crystallization of basaltic melts at > 40 km depth (Ducea, 2002).

The batholith exposed in the Coastal Cordillera above the Cobquecura anomaly may represent the remnants of a continental late Paleozoic volcanic arc. Much of the anomaly lies below the extensive Carboniferous to early Permian age granitoid batholith of the Coastal Cordillera, which intruded a preexisting continental basement (Glodny et al., 2008b), and which may have produced garnet pyroxenite at depth. An anomaly composed of garnet pyroxenite is consistent with the general lack of subsequent volcanism in our central zone, in contrast to the abundance of Mesozoic igneous rocks disrupting the granitoid batholith in our northern zone (Fig. 8C). Models for the development of garnet pyroxenite bodies below arcs indicate that these materials can focus volcanism to neighboring locations and decrease the volume of melt produced (e.g. Karlstrom et al., 2014).

Garnet pyroxenite is stronger than peridotite at temperatures below $< 1200 \, \text{K}$ ($\sim 950 \, ^{\circ}\text{C}$) (Farla et al., 2017) and is not convectively unstable at temperatures below $\sim 500 \, ^{\circ}\text{C}$ (Jull and Kelemen, 2001). As the forearc is well below these temperatures, if the Cobquecura anomaly is a pyroxenite body it would form a rigid backstop that could stabilize this portion of the forearc. This may help explain how the Coastal Cordillera and associated Paleozoic batholith in our central zone has remained stable with a low exhumation rate, suggesting little uplift and erosion, (Glodny et al., 2008a) and no evidence of regional-scale heating since the end of late Triassic rifting (Glodny et al., 2008a).

4.3. The role of large-scale inherited structure in the late Cenozoic development of the Maule forearc

The Bio-Bio Fault marks the northern limit of uplift related to the Arauco Peninsula (Jara-Muñoz et al., 2015) and provides a clear surface expression for the boundary between our central and southern zones. The expression of the boundary between our central and northern zone is much less distinct. The boundary between these two zones may be reflected, as noted in section 4.2, by the presence of Mesozoic plutonic bodies that significantly disrupt the Paleozoic batholith in the northern zone (see Fig. 8B). Additionally, the boundary between these two zones may represent the forearc continuation of the Cortaderas Lineament which has been proposed to mark a significant division within the Chilean and Argentinean Andes (Ramos and Kay, 2006 and references therein; see Fig. 8B). While the Andes in both the regions north and south of the lineament have experienced alternating periods of compression and extension since the Triassic, the region to the south has been characterized by more widespread extension than the region north of the lineament (Ramos and Kay, 2006). If this extension extended to the forearc, it may have acted to help thin the crust in our central zone relative to the northern zone. At least one episode of Oligocene to Miocene extension is documented for the Central Depression section of the forearc south of 36°S (Jordan et al., 2001) and the tapering of the continental crust inboard of our central zone appears to be consistent with this possibility. Alternately, thinning in the central zone may have been a result of the mid-Permian (~275 Ma, Glodny et al., 2006, 2008b) westward displacement of the Carboniferous batholith noted in section 1.

In either case, the pre-Cenozoic, and potentially pre-Mesozoic, tectonics have left the modern Maule forearc broken into three structural zones (see Fig. 9 for schematic summary), the northern two of which center on high velocity, strong bodies at depth. The northern structural zone (Fig. 9A) shows significant evidence for Mesozoic volcanism and ongoing faulting which have largely disrupted pre-Mesozoic structures: the high velocity, strong body at depth in this region is contained within the continental crust and likely represents the deeper portions of the Mesozoic volcanic and plutonic materials exposed at the surface. In the central zone (Fig. 9B) the presence of a strong mantle root retained beneath the Carboniferous batholith in this region may explain why the area has remained stable compared to adjacent areas (Glodny et al., 2006, 2008a, 2008b). The Carboniferous batholith is exposed along a similar orientation at the surface throughout the central and southern zones (compare Fig. 9B and C). However no high velocity body is present at depth in the southern zone (Fig. 9C). Instead, the southern zone shows evidence for extensive basal accretion or underplating of material at the base of the forearc crust (see section 4.1.2 and Haberland et al., 2009). The uplift histories of the batholith in the central and southern zones also differs; within the central zone, the batholith has remained stable since the Triassic while in the southern zone the batholith was stable from the Triassic until ~4 Ma when it began to rapidly uplift (Glodny et al., 2008a).

We propose that the ongoing post-Pliocene uplift in our southern zone associated with the Arauco Peninsula and Arauco Orocline (Glodny et al., 2006; Melnick et al., 2009; Jara-Muñoz et al., 2015) is a product of the removal of a strong body from the forearc mantle beneath this location. While the Carboniferous batholith exposed in the Coastal Cordillera extends south of the Bio-Bio fault, the Cobquecura anomaly that we associate with the batholith's root does not (see Fig. 8B, C). We suggest that a similar root may have previously extended south of the Bio-Bio Fault, extending beneath the continuation of the batholith in the Arauco Orocline up to the Lanalhue Fault. The Lanalhue fault likely truncated this root along with the overlying batholith during Permian left-lateral strike-slip displacement (Glodny et al., 2008b). This root likely acted as a strong block, stabilizing the area throughout the Mesozoic and Cenozoic.

During or immediately before the onset of ~Pliocene uplift in the

Arauco Peninsula and adjacent part of the Arauco Orocline, the strong mantle block detached from the batholith's base and was subsequently displaced at depth away from the trench. This may have occurred as a result of northward migration of a forearc sliver (Melnick et al., 2009) or alternately as a result of complications related to the subduction of the Mocha Fracture Zone (Folguera and Ramos, 2009). Either of these processes could increase the horizontal strain rate in the Arauco mantle block, promoting instability in the high-density root. After detachment, the dense block would sink, or be dragged downward, along with the subducting Nazca oceanic plate. This would simultaneously open space for outer forearc and trench materials to fill, leading to the basal accretion or underplating observed in our RF results in the southern zone and by Haberland et al. (2009) immediately south of our study area. The rapid shift from strong mantle material along the plate interface to relatively weak outer forearc material would change the frictional properties of the plate interface around the Arauco Peninsula relative to the surrounding region, potentially helping to promote uplift (Saillard et al., 2017). A similar process of high-density batholith root removal may be ongoing near the southern edge of the Cobquecura anomaly around the Bio-Bio fault, though we are unable to test this with our current data set.

A root detached from beneath the Arauco Peninsula moving with the Nazca slab eastward relative to the trench would cover the ~100 km distance to the volcanic arc in 1-2 Myrs, given the Nazca plate's present motion eastward with respect to South America (Kendrick et al., 2003, see Fig. 1A). As pyroxenitic root materials can cause distinctive geochemical signatures in arc and back arc volcanism (e.g. Kay and Mpodozis, 2002; Murray et al., 2015), future work examining the last 2-3 Myrs of output from the arc east-northeast of the Arauco Peninsula could test this model. While this model is similar to models of forearc crust removal by subduction erosion in the Central Andes (e.g. Kay and Mpodozis, 2002; Kay and Coira, 2009), we note that the marine forearc in the Arauco region is presently accreting rather than eroding (Contreras-Reyes et al., 2008) and has been accreting since at least the mid-to-late Pliocene (Encinas et al., 2008), concurrent with Arauco uplift. This suggests that the processes affecting the Arauco region differ from subduction erosion in the Central Andes.

5. Conclusions

The Chilean forearc between $\sim 33.5^{\circ}S$ and $\sim 38.5^{\circ}S$ is comprised of three distinct zones (see Figs. 8 and 9): a northern zone between $33.5^{\circ}S$ and $35.5^{\circ}S$ characterized by relatively thick continental crust ($\sim 35-40$ km thick) intersecting the plate interface $\sim 25-30$ km inland from the coast; a central zone between $35.5^{\circ}S$ and $36.5^{\circ}S$ corresponding to thin continental crust (< 25-30 km thick) beneath the Coastal Cordillera which intersects the plate interface at the coast or potentially offshore; and a southern zone between $36.5^{\circ}S$ and $38.5^{\circ}S$ again characterized by relatively thick continental crust ($\sim 35-40$ km thick), possibly thickened by underplating of subducted material, that intersects the plate interface > 30 km inland from the coast.

The previously identified Pichilemu and Cobquecura high velocity anomalies along the Chilean coast have differing relationships with the forearc crust and have separate origins. The Pichilemu anomaly lies within the forearc crust of the northern zone and represents the deep portions of the Paleozoic/Mesozoic batholiths exposed at the surface. The Cobquecura anomaly represents a strong unserpentinized mantle block which forms the core of the central zone at depth. Comparison to prior studies of interseismic locking in the region indicates that the Nazca slab consistently remains coupled to the overriding plate to a depth of $\sim 40-45\,\mathrm{km}$ with little trench parallel variation. A comparison with prior studies of coseismic slip during the 2010 Maule earthquake and subsequent aftershock locations shows that the megathrust ruptured through all three zones to a depth of $\sim 40-45\,\mathrm{km}$, however rupture velocities appear to vary with the northern zone rupturing at a higher velocity than the central or southern zones. The boundary

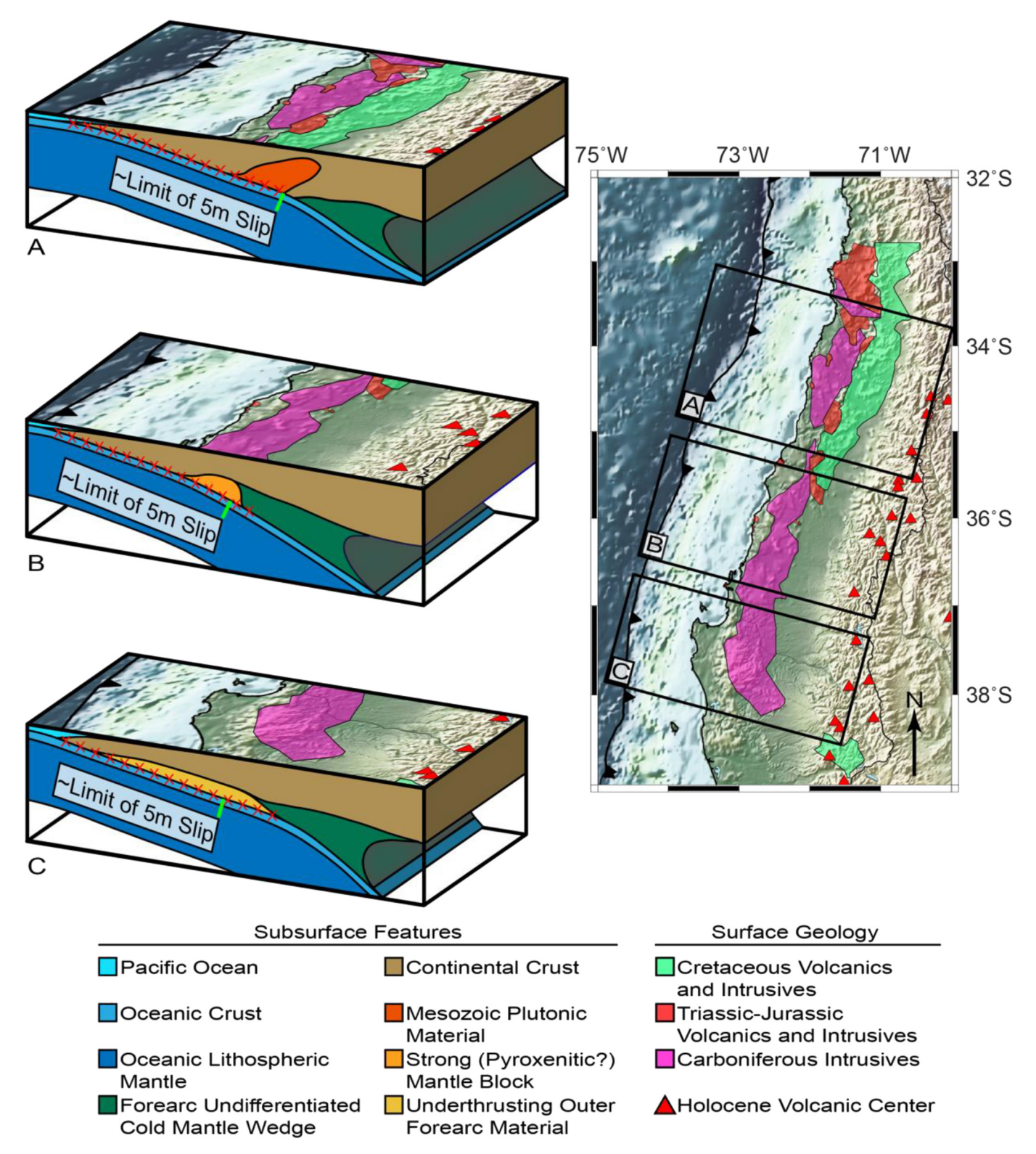


Fig. 9. Schematic block model showing summary of key features in northern (A), central (B), and southern (C) zones mapped in Fig. 8. Red x's mark the approximate extent of the locked megathrust as defined by the 50% contour for the degree of interplate locking (modified from Moreno et al., 2010). Surface exposure of geologic features and Holocene volcanic centers as in Figs. 8 and 1 respectively. Within the northern and southern zones, the locked portion of the megathrust extends nearly to the base of the continental crust. In the central zone, the locked megathrust extends beyond the base of the continental crust to include a block of strong mantle material (the Cobquecura anomaly). In the northern zone, the continental crust contains a block of high velocity material (the Pichilemu anomaly) that represents the continuation of Mesozoic magmatic rocks exposed at the surface. The southern zone around the Arauco Peninsula centers on a wedge-like structure of material being underthrust along the megathrust. See section 4.3 for discussion. (For interpretation of the references to color in this figure legend, the reader is referred to the web version of this article.)

between the northern and central zones corresponds to the Cortaderas Lineament— a major boundary between segments of the Andes in the region since at least the Triassic with the segment north of the lineament experiencing significant contractional deformation and the segment to the south experiencing greater extensional deformation. The boundary between the central and southern zones corresponds to Bio-Bio Fault, the northern boundary of the Arauco Peninsula which has been uplifting since ~4 Ma. The uplift of the Arauco Peninsula may have been driven by the removal of a strong block of mantle material (possibly pyroxenite) similar to that in the Cobquecura region and its replacement by underplated outer forearc materials.

Supplementary data to this article can be found online at https://doi.org/10.1016/j.tecto.2019.228164.

Acknowledgements

Data for this study were downloaded from the Incorporated Research Institutions for Seismology (IRIS) Data Management Center (DMC) located at http://ds.iris.edu. This work was supported by NSF grant EAR-1415914. B. Bishop was also supported by: UA Graduate College Scholarship and a ChevronTexaco Geology Fellowship. We thank Dietrich Lange of the University of Potsdam for sharing aftershock hypocenter locations for the 2010 Maule earthquake along with Kelin Wang and an anonymous reviewer for providing comments which have greatly strengthened this paper.

References

- Abers, G.A., Hacker, B.R., 2016. A MATLAB toolbox and Excel workbook for calculating densities, seismic wave speeds, and major element composition of minerals and rocks at pressure and temperature. Geochem. Geophys. Geosyst. 17, 616–624. https://doi. org/10.1002/2015GC006171.
- Abers, G.A., van Keken, P.E., Hacker, B.R., 2017. The cold and relatively dry nature of mantle forearcs in subduction zones. Nat. Geosci. 10, 333–337. https://doi.org/10. 1038/ngeo2922.
- Aron, F., Cembrano, J., Astudillo, F., Allmendinger, R.W., Arancibia, G., 2015. Constructing forearc architecture over megathrust seismic cycles: geological snapshots from the Maule earthquake region, Chile. Geol. Soc. Am. Bull. 127 (3/4), 464–479. https://doi.org/10.1130/B31125.1.
- Becerra, J., Contreras-Reyes, E., Arriagada, C., 2013. Seismic structure and tectonics of the southern Arauco Basin, south-central Chile (~38°S). Tectonophysics 592, 53–66. https://doi.org/10.1016/j.tecto.2013.02.012.
- Beck, S., Barrientos, S., Kausel, E., Reyes, M., 1998. Source characteristics of historic earthquakes along the central Chile subduction zone. J. S. Am. Earth Sci. 11 (2), 115–129. https://doi.org/10.1016/S0895-9811(98)00005-4.
- Beck, S., Wallace, T., Zandt, G., 2000. Slab Geometry in the Southern Andes (Data Set): International Federation of Digital Seismograph Networks. https://doi.org/10.7914/ SN/YC 2000
- Charrier, R., Pinto, L., Pía Rodríguez, M., 2007. Tectonostratigraphic evolution of the Andean Orogen in Chile. In: Moreno, T., Gibbons, W. (Eds.), The Geology of Chile. The Geological Society, London, United Kingdom, pp. 22–114. https://doi.org/10. 1144/GOCH.3.
- Clift, P., Vannucchi, P., 2004. Controls on tectonic accretion versus erosion in subduction zones: Implications for the origin and recycling of the continental crust. Reviews of Geophysics 42, RG2001. https://doi.org/10.1029/2003RG000127.
- Comte, D., Eisenberg, A., Lorca, E., Pardo, M., Ponce, L., Saragoni, R., Singh, S.K., Suárez, 1986. The 1985 central Chile earthquake: a repeat of previous great earthquakes in the region? Science 233, 449–453. https://doi.org/10.1126/science.233.4762.449.
- Contreras-Reyes, E., Grevemeyer, I., Flueh, E.R., Reichert, C., 2008. Upper lithospheric structure of the subduction zone offshore of southern Arauco peninsula, Chile, at ~38°S. Journal of Geophysical Research Solid Earth 113, B07303. https://doi.org/
- Contreras-Reyes, E., Flueh, E.R., Grevemeyer, I., 2010. Tectonic control on sediment accretion and subduction off south central Chile: implications for coseismic rupture processes of the 1960 and 2010 megathrust earthquakes. Tectonics 29, TC6018. https://doi.org/10.1029/2010TC002734.
- Contreras-Reyes, E., Becerra, J., Kopp, H., Reichert, C., Díaz-Naveas, J., 2014. Seismic structure of the north-central Chilean convergent margin: Subduction erosion of a paleomagmatic arc. Geophys. Res. Lett. 41, 1523–1529. https://doi.org/10.1002/ 2013GL058729.
- Contreras-Reyes, E., Maksymowicz, A., Lang, D., Grevemeyer, I., Muñoz-Linford, P., Moscoso, E., 2017. On the relationship between structure, morphology and large coseismic slip: a case study of the M_w 8.8 Maule, Chile 2010 earthquake. Earth Planet. Sci. Lett. 478, 27–39. https://doi.org/10.1016/j.epsl.2017.08.028.
- Dannowski, A., Grevemeyer, I., Kraft, H., Arroyo, I., Thorwart, M., 2013. Crustal thickness and mantle wedge structure from receiver functions in the Chilean Maule region at 35°S. Tectonophysics 592, 159–164. https://doi.org/10.1016/j.tecto.2013.02.015.
- Delouis, B., Nocquet, J.-M., Vallée, M., 2010. Slip distribution of the February 27, 2010 Mw = 8.8 Maule earthquake, central Chile, from static and high-rate GPS, InSAR, and broadband teleseismic data. Geophys. Res. Lett. 37, L17305. https://doi.org/10.

1029/2010GL043899.

- Ducea, M.N., 2002, Constraints on the bulk composition and root foundering rates of continental arcs: A California arc perspective: Journal of Geophysical Research Solid Earth, v. 107, no. B11, p. ECV 15-1—ECV 15-13, doi:https://doi.org/10.1029/ 2001JB000643.
- Dueker, K.G., Sheehan, A.F., 1997. Mantle discontinuities structure from midpoint stacks of converted P to S waves across the Yellowstone hotspot track. J. Geophys. Res. 102, 8313–8327. https://doi.org/10.1029/96JB03857.
- Duputel, Z., Rivera, L., Kanamori, H., Hayes, G., 2012. W phase source inversion for moderate to large earthquakes (1990–2010). Geophys. J. Int. 189, 1125–1147. https://doi.org/10.1111/j.1365-246X.2012.05419.x.
- Dura, T., Horton, B.P., Cisternas, M., Ely, L.L., Hong, I., Nelson, A.R., Wesson, R.L., Pilarczyk, J.E., Parnell, A.C., Nikitina, D., 2017. Subduction zone slip variability during the last millennium, south-central Chile. Quat. Sci. Rev. 175, 112–137. https://doi.org/10.1016/j.quascirev.2017.08.023.
- Encinas, A., Finger, K.L., Nielsen, S.N., Lavenu, A., Buatois, L.A., Peterson, D.E., Le Roux, J.P., 2008. Rapid and major coastal subsidence during the late Miocene in south-central Chile. J. S. Am. Earth Sci. 25, 157–175. https://doi.org/10.1016/j.jsames. 2007.07.001.
- Farías, M., Comte, D., Charrier, R., Martinod, J., David, C., Tassara, A., Tapia, F., Fock, A., 2010a. Crustal-scale structure architecture in central Chile based on seismicity and surface geology: Implications for Andean mountain building. Tectonics 29, TC3006. https://doi.org/10.1029/2009TC002480.
- Farías, M., Vargas, G., Tassara, A., Carretier, S., Baize, S., Melnick, D., Bataille, K., 2010b. Land-level changes produced by the M_W 8.8 210 Chilean earthquake. Science 329, 916. https://doi.org/10.1126/science.1192094.
- Farla, R., Rosenthal, A., Bollinger, C., Petitgirard, S., Guignard, J., Miyajima, N., Kawazoe, T., Crichton, W.A., Frost, D.J., 2017. High-pressure, high-temperature deformation of dunite, eclogite, clinopyroxenite and garnetite using in situ X-ray diffraction. Earth Planet. Sci. Lett. 473, 291–302. https://doi.org/10.1016/j.epsl.2017. 06.019
- Ferrand, T.P., Hilairet, N., Incel, S., Deldicque, D., Labrousse, L., Gasc, J., Renner, J., Wang, Y., Green II, H.W., Schubnel, A., 2017. Dehydration-driven stress transfer triggers intermediate-depth earthquakes. Nat. Commun. 8 (15247). https://doi.org/10.1038/ncomms15247.
- Folguera, A., Ramos, V.A., 2009. Collision of the Mocha fracture zone and a < 4 Ma old wave of orogenic uplift in the Andes (36°–38°S). Lithosphere 1 (6), 364–369. https://doi.org/10.1130/166.1
- Frassetto, A., Thybo, H., 2013. Receiver function analysis of the crust and upper mantle in Fennoscandia isostatic implications. Earth Planet. Sci. Lett. 381, 234–246. https://doi.org/10.1016/j.epsl.2013.07.001.
- Frassetto, A.M., Zandt, G., Gilbert, H., Owens, T.J., Jones, C.H., 2011. Structure of the Sierra Nevada from receiver functions and implications for lithospheric foundering. Geosphere 7 (4), 898–921. https://doi.org/10.1130/GES00570.1.
- Gao, X., Wang, K., 2017. Rheological separation of the megathrust seismogenic zone and episodic tremor and slip. Nature 543, 416–419. https://doi.org/10.1038/ nature21389
- Gilbert, H., Beck, S., Zandt, G., 2006. Lithospheric and upper mantle structure of central Chile and Argentina. Geophysics Journal International 165, 383–398. https://doi. org/10.1111/j.1365-246X.2006.02867.x.
- Global Volcanism Program, 2013, Volcanoes of the World, v. 4.5.0: Washington, D.C., Smithsonian Institution, doi:https://doi.org/10.5479/si.GVP.VOTW5-2013 (accessed September 2016).
- Glodny, J., Echtler, H., Figueroa, O., Franz, G., Gräfe, K., Kemnitz, H., Kramer, W., Krawczyk, C., Lohrmann, J., Lucassen, F., Melnick, D., Rosenau, M., Seifert, W., 2006. Long-term geological evolution and mass-flow balance of the south-central Andes. In: Oncken, O., Chong, G., Franz, G., Giese, P., Götze, H.-J., Ramos, V.A., Strecker, M.R., Wigger, P. (Eds.), The Andes: Active Subduction Orogeny. Springer-Verlag, Berlin Heidelberg, Germany, pp. 401–428. https://doi.org/10.1007/978-3-540-48684-8 19.
- Glodny, J., Gräfe, K., Echtler, H., Rosenau, M., 2008a. Mesozoic to Quaternary continental margin dynamics in south-central Chile (36-42°S): the apatite and zircon fission track perspective. Int. J. Earth Sci. 97, 1271–1291. https://doi.org/10.1007/s00531-007-0203-1.
- Glodny, J., Echtler, H., Collao, S., Ardiles, M., Burón, P., Figueroa, O., 2008b. Differential late Paleozoic active margin evolution in south-central Chile (37°S–40°S) the Lanalhue Fault Zone. J. S. Am. Earth Sci. 26, 397–411. https://doi.org/10.1016/j.isames.2008.06.001.
- Groß, K., Micksch, U., TIPTEQ Research Group, Seismics Team, 2008. The reflection seismic survey of project TIPTEQ—the inventory of the Chilean subduction zone at 38.2°S. Geophysics Journal International 172, 565–571. https://doi.org/10.1111/j. 1365-246X.2007.03680.x.
- Haberland, C., Rietbrock, A., Lange, D., Bataille, K., and Dahm, T., 2009, Structure of the seismogenic zone of the southcentral Chilean margin revealed by local earthquake traveltime tomography: Journal of Geophysical Research, 114, B01317, doi:https:// doi.org/10.1029/2008JB005802.
- Hasegawa, A., Nakajima, J., 2017. Seismic imaging of slab metamorphism and genesis of intermediate-depth intraslab earthquakes. Progress in Earth and Planetary Science 4. https://doi.org/10.1186/s40645-017-0126-9.
- Hasegawa, A., Horiuchi, S., Umino, N., 1994. Seismic structure of the northeastern Japan convergent margin: a synthesis. J. Geophys. Res. 99, 22295–22311. https://doi.org/ 10.1029/93JB02797.
- Hayes, G.P., Moore, G.L., Portner, D.E., Hearne, M., Flamme, H., Furtney, M., Smoczyk, G.M., 2018. Slab2, a comprehensive subduction zone geometry model. Science 362, 58–61. https://doi.org/10.1126/science.aat4723.
- Heit, B., Yuan, X., Bianchi, M., Sodoudi, F., Kind, R., 2008. Crustal thickness estimation beneath the southern central Andes at 30°S and 36°S from S wave receiver function analysis. Geophysics Journal International 174, 249–254. https://doi.org/10.1111/j. 1365-246X.2008.03780.x.
- Hervé, F., 1988. Late Paleozoic subduction and accretion in southern Chile. Episodes 11

(3), 183-188.

- Hervé, F., Calderón, M., Fanning, C.M., Pankhurst, R.J., Godoy, E., 2013. Provenance variations in the late Paleozoic accretionary complex of central Chile as indicated by detrital zircons. Gondwana Res. 23, 1122–1135. https://doi.org/10.1016/j.gr.2012.06.016
- Hicks, S.P., Rietbrock, A., Haberland, C.A., Ryder, I.M.A., Simons, M., Tassara, A., 2012. The 2010 M_w 8.8 Maule, Chile earthquake: Nucleation and rupture propagation controlled by a subducted topographic high. Geophys. Res. Lett. 39, L19308. https://doi.org/10.1029/2012GL053184.
- Hicks, S.P., Rietbrock, A., Ryder, I.M.A., Lee, C.-S., Miller, M., 2014. Anatomy of a megathrust: the 2010 M8.8 Maule, Chile earthquake rupture zone imaged using seismic tomography. Earth Planet. Sci. Lett. 405, 142–155. https://doi.org/10.1016/ i.ensl.2014.08.028
- Huang, Y.L., Hwang, R.D., Jhuang, Y.S., Lin, C.Y., 2017. Rupture features of the 2010 Mw 8.8 Chile earthquake extracted from surface waves. 69, 41. https://doi.org/10.1186/ s40623.017-0624-4
- Hyndman, R.D., Wang, K., 1993. Thermal constraints on the zone of major thrust earthquake failure: the Cascadia Subduction Zone. Journal of Geophysical Research Solid Earth 98, 2039–2060. https://doi.org/10.1029/92JB02279.

 Hyndman, R.D., Wang, K., Yamano, M., 1995. Thermal constraints on the seismogenic
- Hyndman, R.D., Wang, K., Yamano, M., 1995. Thermal constraints on the seismogenic portion of the southwestern Japan subduction thrust. Journal of Geophysical Research Solid Earth 100, 15373–15392. https://doi.org/10.1029/95JB00153.
- Institut de Physique du Globe de Paris (IPGP) and École ed Observatoire des Sciences de la Terre de Strasbourg (EOST), 1982. GEOSCOPE, French Global Network of Broadband Seismic Stations (Version 0) (Data Set). Institut de Physique du Globe de Paris (IPGP) https://doi.org/10.18715/geoscope.g.
- Jara-Muñoz, J., Melnick, D., Brill, D., Strecker, M.R., 2015. Segmentation of the 2010 Maule Chile earthquake rupture from a joint analysis of uplifted marine terraces and seismic-cycle deformation. Quat. Sci. Rev. 113, 171–192. https://doi.org/10.1016/j. quascirev.2015.01.005.
- Jordan, T.E., Burns, W.M., Veiga, R., Pángaro, F., Copeland, P., Kelley, S., Mpodozis, C., 2001. Extension and basin formation in the southern Andes caused by increased convergence rate: a mid-Cenozoic trigger for the Andes. Tectonics 20, 308–324. https://doi.org/10.1029/1999TC001181.
- Jull, M., Kelemen, P.B., 2001. On the conditions for lower crustal convective instability. J. Geophys. Res. 106, 6423–6446. https://doi.org/10.1029/2000JB900357.
- Karlstrom, L., Lee, C.-T.A., Manga, M., 2014. The role of magmatically driven lithospheric thickening on arc front migration. Geochem. Geophys. Geosyst. 15, 2655–2675. https://doi.org/10.1002/2014GC005355.
- https://doi.org/10.1002/2014GC005355.

 Kato, A., Iidaka, T., Ikuta, R., Yoshida, Y., Katsumata, K., Iwasaki, T., Sakai, S., Thurber, C., Tsumura, N., Yamaoka, K., Watanabe, T., Kunitomo, T., Yamazaki, F., Okubo, M., Suzuki, S., and Hirata, N., 2010, Variations of fluid pressure within the subducting oceanic crust and slow earthquakes: Geophysical Research Letters, 27, L14310, doi:https://doi.org/10.1029/2010GL043723.
- Kay, S.M., Coira, B.L., 2009. Shallowing and steepening subduction zones, continental lithospheric loss, magmatism, and crustal flow under the central Andean Altiplano-Puna Plateau. In: Kay, S.M., Ramos, V.A., Dickinson, W.R. (Eds.), Backbone of the Americas: Shallow Subduction, Plateau Uplift, and Ridge and Terrane Collision. 204. Geological Society of America Memoir, pp. 229–259. https://doi.org/10.1130/2009.
- Kay, S.M., Mpodozis, C., 2002. Magmatism as a probe to the Neogene shallowing of the Nazca plate beneath the modern Chilean flat-slab. J. S. Am. Earth Sci. 15, 39–57. https://doi.org/10.1016/S0895-9811(02)00005-6.
- Kendrick, E., Bevis, M., Smalley Jr., R., Brooks, B., Barriga Vargas, R., Laurie, E., Souto Fortes, L.P., 2003. The Nazca-South America Euler vector and its rate of change. J. S. Am. Earth Sci. 16, 125–131. https://doi.org/10.1016/S0895-9811(03)00028-2.
- Kiser, E., Ishii, M., 2011. The 2010 Mw 8.8 Chile earthquake: triggering on multiple segments and frequency-dependent rupture behavior. Geophys. Res. Lett. 38, L07301. https://doi.org/10.1029/2011GL047140.
- Koper, K.D., Hutko, A.R., Lay, T., Sufri, O., 2012. Imaging short-period seismic radiation from the 27 February 2010 Chile (M_W 8.8) earthquake by back-projection of P, PP, and PKIKP waves. J. Geophys. Res. 117, B02308. https://doi.org/10.1029/ 2011JB008576.
- Lange, D., Tilmann, F., Barrientos, S.E., Contreras-Reyes, E., Methe, P., Moreno, M., Heit, B., Agurto, H., Bernard, P., Vilotte, J.-P., Beck, S., 2012. Aftershock seismicity of the 27 February 2010 Mw 8.8 Maule earthquake. Earth Planet. Sci. Lett. 317–318, 413–425. https://doi.org/10.1016/j.epsl.2011.11.034.
- Lee, C.-T.A., Anderson, D.L., 2015. Continental crust formation at arcs, the arclogite "delamination" cycle, and one origin for fertile melting anomalies in the mantle. Science Bulletin 60, 1141–1156. https://doi.org/10.1007/s11434-015-0828-6.
- Ligorría, J.P., Ammon, C.J., 1999. Iterative Deconvolution and Receiver-function Estimation. 89. Bulletin of the Seismological Society of America, pp. 1395–1400.
- Lorito, S., Romano, F., Atzori, S., Tong, X., Avallone, A., McCloskey, J., Cocco, J., Boschi, E., Piatanesi, A., 2011. Limited overlap between the seismic gap and coseismic slip of the great 2010 Chile earthquake. Nat. Geosci. 4, 173–177. https://doi.org/10.1038/NGE01073.
- Melnick, D., 2016. Rise of the central Andean coast by earthquakes straddling the Moho. Nat. Geosci. 9, 401–407. https://doi.org/10.1038/ngeo2683.
- Melnick, D., Bookhagen, B., Strecker, M.R., Echtler, H.P., 2009. Segmentation of megathrust rupture zones from fore-arc deformation patterns over hundreds to millions of years, Arauco peninsula, Chile. Journal of Geophysical Research Solid Earth 114, B01407. https://doi.org/10.1029/2008JB005788.
- Métois, M., Socquet, A., Vigny, C., 2012. Interseismic coupling, segmentation and mechanical behavior of the central Chile subduction zone. Journal of Geophysical Research Solid Earth 117, B03406. https://doi.org/10.1029/2011JB008736.
- Mitchell, E.K., Fialko, Y., Brown, K.M., 2015. Frictional properties of gabbro at conditions

- corresponding to slow slip events in subduction zones. Geochem. Geophys. Geosyst. 16, 4006–4020. https://doi.org/10.1002/2015GC006093.
- Mordojovich, C., 1981. Sedimentary basins of Chilean Pacific offshore. In: Halbouty, M.T. (Ed.), Energy Resources of the Pacific Region. The American Association of Petroleum Geologists, Tulsa, U.S.A., pp. 63–82. https://doi.org/10.1306/St12420C7.
- Moreno, M., Rosenau, Oncken, O., 2010. 2010 Maule earthquake slip correlates with preseismic locking of Andean subduction zone. Nature 467, 198–202. https://doi.org/10.1038/nature09349.
- Moreno, M., Melnick, D., Rosenau, M., Baez, J., Klotz, J., Oncken, O., Tassara, A., Chen, J., Bataille, K., Bevis, M., Socquet, A., Bolte, J., Vigny, C., Brooks, B., Ryder, I., Grund, V., Smalley, B., Carrizo, D., Bartsch, M., Hase, H., 2012. Toward understanding tectonic control on the Mw. 8.8 2010 Maule Chile earthquake. Earth Planet. Sci. Lett. 321–322, 152–165. https://doi.org/10.1016/j.epsl.2012.01.006.
- Murray, K.E., Ducea, M.N., Schoenbohm, L., 2015. Foundering-driven lithospheric melting: the central Andean mafic lavas on the Puna Plateau (22°S–27°S). In: DeCelles, P.G., Ducea, M.N., Carrapa, B., Kapp, P.A. (Eds.), Geodynamics of a Cordilleran Orogenic System: The Central Andes of Argentina and Northern Chile. 212 Geological Society of America Memoir. https://doi.org/10.11130/2015. 1212(08).
- Nakajima, J., Matsuzawa, T., Hasegawa, A., 2002. Moho depth variations in the central part of northeastern Japan estimated from reflected and converted waves. Phys. Earth Planet. Inter. 130, 31-47. https://doi.org/10.1016/S0031-9201(01)00307-7.
- Peng, Z., Gomberg, J., 2010. An integrated perspective of the continuum between earthquakes and slow-slip phenomena. Nat. Geosci. 3, 599–607. https://doi.org/10. 1038/NGE0940.
- Ramos, V.A., Kay, S.M., 2006. Overview of the tectonic evolution of the southern central Andes of Mendoza and Neuquén (35°-39°S latitude). In: Kay, S.M., Ramos, V.A. (Eds.), Evolution of an Andean Margin: Tectonic and Magmatic View from the Andes to the Neuquén Basin (35°-39°S). Geological Society of America Special Paper 407pp. 1–18. https://doi.org/10.1130/2006.2407(01).
- Rehak, K., Strecker, M.R., Echtler, H.P., 2008. Morphotectonic segmentation of an active forearc, 37°–41°S, Chile. Geomorphology 94, 98–116. https://doi.org/10.1016/j. geomorph.2007.05.002.
- Reynard, B., 2013. Serpentine in active subduction zones. Lithos 178, 171–185. https://doi.org/10.1016/j.lithos.2012.10.012.
- Roecker, S., Russo, R., 2010. RAMP Response for 2010 Earthquake (Dataset). International Federation of Digital Seismograph Networkshttps://doi.org/10.7914/ SN/XY 2010.
- Rondenay, S., Abers, G.A., van Keken, P.E., 2008. Seismic imaging of subduction zone metamorphism. Geology 36, 275–278. https://doi.org/10.1130/G24112A.1.
- Ryan, J., Beck, S., Zandt, G., Wagner, L., Minaya, E., Tavera, H., 2016. Central Andean crustal structure from receiver function analysis. Tectonophysics 682, 120–133. https://doi.org/10.1016/j.tecto.2016.04.048.
- Rychert, C.A., Rondenay, S., Fischer, K.M., 2007. P-to-S and S-to-P imaging of a sharp lithosphere-asthenosphere boundary beneath eastern North America. J. Geophys. Res. 112, B08314. https://doi.org/10.1029/2006JB004619.
- Saillard, M., Audin, L., Rousset, B., Avouac, J.-P., Chlieh, M., Hall, S.R., Husson, L., Farber, D.L., 2017. From the seismic cycle to long-term deformation: linking seismic coupling and Quaternary coastal geomorphology along the Andean megathrust. Tectonics 36, 241–256. https://doi.org/10.1002/2016TC004156.
- Sheehan, A.F., Shearer, P.M., Gilbert, H.J., Dueker, K.G., 2000. Seismic migration processing of P-SV converted phases from mantle discontinuity structure beneath the Snake River Plain, western United States. J. Geophys. Res. 105, 19,055–19,065. https://doi.org/10.1029/2000JB900112.
- Van Keken, P.E., Hacker, B.R., Syracuse, E.M., Abers, G.A., 2011. Subduction factory: 4. Depth-dependent flux of H₂O from subducting slabs worldwide. Journal of Geophyiscal Research 116, B01401. https://doi.org/10.1029/2010JB007922.
- Vilotte, J.-P., RESIF, 2011. Seismic Network XS:CHILE MAULE Aftershock Temporary Experiment (RESIF-SISMOB) (Version 0) (Data Set). RESIF- Réseau Seismologique et géodésique Françaishttps://doi.org/10.15778/resif.xs2010.
 Völker, D., Stipp, M., 2015. Water input and water release from the subducting Nazca
- Völker, D., Stipp, M., 2015. Water input and water release from the subducting Nazca Plate along southern central Chile (33°S-46°S). Geochem. Geophys. Geosyst. 16, 1825–1847. https://doi.org/10.1002/2015GC005766.
- Wang, K., Tréhu, A.M., 2016. Invited review paper: some outstanding issues in the study of great megathrust earthquakes—the Cascadia example. J. Geodyn. 98, 1–18. https://doi.org/10.1016/j.jog.2016.03.010.
- Wang, J., Zhao, D., Yao, Z., 2017. Seismic anisotropy evidence for dehydration embrittlement triggering intermediate-depth earthquakes. Sci. Rep. 7 (2613). https://doi. org/10.1038/s41598-017-02563-w.
- Ward, K.M., Porter, R.C., Zandt, G., Beck, S.L., Wagner, L.S., Minaya, E., Tavera, H., 2013.
 Ambient noise tomography across the central Andes. Geophys. J. Int. 194,
 1559–1573. https://doi.org/10.1093/gij/ggt1166
- 1559–1573. https://doi.org/10.1093/gji/ggt166.
 Willner, A.P., Richter, P.P., Ring, U., 2009. Structural overprint of a late Paleozoic accretionary system in north-central Chile (34°–35°S) during post-accretional deformation. Andean Geol. 36 (1), 17–36.
- Yuan, X., Sobolev, S.V., Kind, R., Oncken, O., Bock, G., Asch, G., Schurr, B., Graeber, F., Rudloff, A., Hanka, W., Wylegalla, K., Tibi, R., Haberland, C., Rietbrock, A., Giese, P., Wigger, P., Röwer, P., Zandt, G., Beck, S., Wallace, T., Pardo, M., Comte, D., 2000. Subduction and collision processes in the central Andes constrained by converted seismic phases. Nature 408, 958–961. https://doi.org/10.1038/35050073.
- Yue, H., Lay, T., Rivera, L., An, C., Vigny, C., Tong, X., Báez Soto, J.C., 2014. Localized fault slip to the trench in the 2010 Maule, Chile $M_W=8.8$ earthquake from joint inversion of high-rate GPS, teleseismic body waves, InSAR, campaign GPS, and tsunami observations. Journal of Geophysical Research Solid Earth 119, 7786–7804. https://doi.org/10.1002/2014JB011340.